Brain, Behavior, and Immunity 82 (2019) 406–421

Contents lists available at ScienceDirect

Brain, Behavior, and Immunity

journal homepage: www.elsevier.com/locate/ybrbi

Full-length Article

Murine iPSC-derived microglia and macrophage cell culture models recapitulate distinct phenotypical and functional properties of classical and alternative neuro-immune polarisation

Alessandra Quarta[a,b], Debbie Le Blon[a,b], Tine D'aes[a,b], Zoë Pieters[b,c,g], Somayyeh Hamzei Taj[d], Francesc Miró-Mur[e], Evi Luyckx[a,b,f], Elise Van Breedam[a,b], Jasmijn Daans[a,b], Herman Goossens[b], Sylvia Dewilde[f], Niel Hens[b,c,g], Vincent Pasque[h], Anna M. Planas[e,i], Mathias Hoehn[d,j], Zwi Berneman[a,b], Peter Ponsaerts[a,b,*]

[a] *Laboratory of Experimental Hematology, University of Antwerp, Antwerp, Belgium*
[b] *Vaccine and Infectious Disease Institute (Vaxinfectio), University of Antwerp, Antwerp, Belgium*
[c] *Interuniversity Institute for Biostatistics and Statistical Bioinformatics, Hasselt University, Belgium*
[d] *In-vivo-NMR Laboratory, Max Planck Institute for Metabolism Research, Cologne, Germany*
[e] *Institut d'Investigacions Biomèdiques August Pi i Sunyer (IDIBAPS), Barcelona, Spain*
[f] *Protein Chemistry, Proteomics and Epigenetic Signaling, University of Antwerp, Antwerp, Belgium*
[g] *Centre for Health Economics Research and Modelling Infectious Diseases, University of Antwerp, Belgium*
[h] *Department of Development and Regeneration, Leuven Stem Cell Institute, Leuven Cancer Institute, KU Leuven – University of Leuven, Belgium*
[i] *Department of Brain Ischemia and Neurodegeneration, Institut d'Investigacions Biomèdiques de Barcelona (IIBB)-Consejo Superior de Investigaciones Científicas (CSIC), Barcelona, Spain*
[j] *Department of Radiology, Leiden University Medical Center, Leiden, Netherlands*

ARTICLE INFO

Keywords:
iPSC
Microglia
Macrophages
Stroke
Neuroinflammation
Interleukin (IL) 13
Polarisation
Classical activation
Alternative activation

ABSTRACT

The establishment and validation of reliable induced pluripotent stem cell (iPSC)-derived *in vitro* models to study microglia and monocyte/macrophage immune function holds great potential for fundamental and translational neuro-immunology research. In this study, we first demonstrate that ramified CX_3CR1^+ iPSC-microglia (cultured within a neural environment) and round-shaped CX_3CR1^- iPSC-macrophages can easily be differentiated from newly established murine $CX_3CR1^{eGFP/+}CCR2^{RFP/+}$ iPSC lines. Furthermore, we show that obtained murine iPSC-microglia and iPSC-macrophages are distinct cell populations, even though iPSC-macrophages may upregulate CX_3CR1 expression when cultured within a neural environment. Next, we characterized the phenotypical and functional properties of murine iPSC-microglia and iPSC-macrophages following classical and alternative immune polarisation. While iPSC-macrophages could easily be triggered to adopt a classically-activated or alternatively-activated phenotype following, respectively, lipopolysaccharide + interferon γ or interleukin 13 (IL13) stimulation, iPSC-microglia and iPSC-macrophages cultured within a neural environment displayed a more moderate activation profile as characterised by the absence of MHCII expression upon classical immune polarisation and the absence of Ym1 expression upon alternative immune polarisation. Finally, extending our preceding *in vivo* studies, this striking phenotypical divergence was also observed for resident microglia and infiltrating monocytes within highly inflammatory cortical lesions in $CX_3CR1^{eGFP/+}CCR2^{RFP/+}$ mice subjected to middle cerebral arterial occlusion (MCAO) stroke and following IL13-mediated therapeutic intervention thereon. In conclusion, our study demonstrates that the applied murine iPSC-microglia and iPSC-macrophage culture models are able to recapitulate *in vivo* microglia and monocyte/macrophage ontogeny and corresponding phenotypical/functional properties upon classical and alternative immune polarisation, and therefore represent a valuable *in vitro* platform to further study and modulate microglia and (infiltrating) monocyte immune responses under neuro-inflammatory conditions within a neural environment.

* Corresponding author at: Laboratory of Experimental Hematology, Vaccine and Infectious Disease Institute (Vaxinfectio), University of Antwerp, Campus Drie Eiken (CDE-S6.51), Universiteitsplein 1, 2610 Antwerp (Wilrijk), Belgium.
E-mail address: peter.ponsaerts@uantwerpen.be (P. Ponsaerts).

https://doi.org/10.1016/j.bbi.2019.09.009
Received 7 June 2019; Received in revised form 5 September 2019; Accepted 12 September 2019
Available online 13 September 2019

1. Introduction

Neuroinflammation is the response of the central nervous system (CNS) to disturbed homeostasis and is a hallmark of all neurological disorders, including developmental, traumatic, infectious and neurodegenerative diseases (DiSabato et al., 2016). Following neurotrauma, resident microglia and infiltrating monocytes co-orchestrate the pathological environment and can either contribute to disease progression or promote protection and/or regeneration depending on their activation status (Kanazawa et al., 2017; Kong and Gao, 2017; Kronenberg et al., 2018; Kumar et al., 2016; Milich et al., 2019; Yamasaki et al., 2014). Microglia and monocyte/macrophage activation states are generally situated between two spectral ends of functional polarisation: 'classical activation' which is associated with the secretion of pro-inflammatory molecules contributing to deleterious effects and 'alternative activation' which is associated with the secretion of immune-modulating (anti-inflammatory) mediators as well as neurotrophic factors. Furthermore, immune polarized microglia and monocytes/macrophages are not locked in a particular state and their function can be altered upon changes in the neuro-inflammatory environment (Italiani and Boraschi, 2014; Mosser and Edwards, 2008; Murray, 2017; Orihuela et al., 2016; Ransohoff and Perry, 2009; Smith et al., 2016). Within the context of neuro-inflammatory disease, forced alternative activation of resident microglia and infiltrating monocytes is therefore expected to become a new therapeutic approach (Cherry et al., 2014; Gupta et al., 2018; Hu et al., 2015; Kanazawa et al., 2017; Rajkovic et al., 2018). However, one should realize that the concept and functional consequences of alternative immune polarisation may be different for microglia and infiltrating monocytes, especially as both immune cell populations are of distinct embryonic origin (Ginhoux et al., 2010; Ginhoux and Jung, 2014; Kierdorf et al., 2013; Prinz and Priller, 2014; Schulz et al., 2012).

The *in vivo* study of differential neuro-immune effector functions by microglia and infiltrating monocytes during neuroinflammatory events requires complex experimental setups, including bone marrow chimeric mice and transgenic mouse models (Koeniger and Kuerten, 2017). Of specific interest is the $CX_3CR1^{eGFP/+}CCR2^{RFP/+}$ reporter gene transgenic mouse model as an experimental tool to distinguish CX_3CR1^{+} microglia, labelled with the enhanced green fluorescent protein (eGFP), from $CCR2^{+}$ infiltrating monocytes, of which the majority is labelled with the red fluorescent protein (RFP) (Saederup et al., 2010). Using this model, we have previously documented the contribution and activation profile of both microglia and infiltrating monocytes in mice following cuprizone (CPZ)-induced CNS inflammation and demyelination (Le Blon et al., 2016), spinal cord injury (SCI) (Dooley et al., 2016) and middle cerebral artery occlusion (MCAO)-induced stroke (Hamzei Taj et al., 2018). Although there are obvious model-dependent differences in spatial and numeric contribution of activated microglia and infiltrating monocytes in the inflamed lesions, one relevant functional difference we already described was that upregulation of MHCII was more restricted to the infiltrating monocyte population as compared to the microglia population (Dooley et al., 2016; Hamzei Taj et al., 2018; Le Blon et al., 2016). In addition, we investigated in these mouse models whether therapeutic administration of the immune-modulating cytokine interleukin 13 (IL13), either by lentiviral vector injection or by implantation of genetically engineered mesenchymal stem cells (MSC), could enhance the appearance of the alternatively activated phenotype in microglia and infiltrating monocytes, as well as whether this intervention could affect disease outcome. While this therapeutic approach was highly successful in terms of histopathological and - to a certain extent - functional recovery, we also observed that the forced induction of immune cell phenotypes associated with alternative activation, as characterised by the upregulation of Arginase-1 expression, was significantly more efficient in infiltrating monocytes as compared to microglia (Dooley et al., 2016; Hamzei Taj et al., 2018; Le Blon et al., 2016). These observations have clear implications for the further development of therapeutic strategies aiming at converting a classical pro-inflammatory CNS environment into an alternative activated and/or regeneration-promoting environment and highlight the need for a more profound investigation of the immune polarization potential of both microglia and monocytes/macrophages. In this context, the existence of reliable *in vitro* cell culture models to study and modulate neuro-inflammatory responses will be of great benefit.

Reliable *in vitro* modelling of neuroinflammatory responses is indeed one of the major challenges in current biomedical research and it is expected that cell culture systems that accurately mimic inflammation-induced pathology will become essential tools for the preclinical development and validation of novel therapies to treat central nervous system (CNS) injury or disease. During the past years, significant efforts were devoted to generating genuine microglia from induced pluripotent stem cells (iPSC), resulting in the description of several protocols to obtain iPSC-derived microglia-like cell populations for profound *in vitro* studies (Abud et al., 2017; Beutner et al., 2010; Brownjohn et al., 2018; Claes et al., 2019; Douvaras et al., 2017; Etemad et al., 2012; Garcia-Reitboeck et al., 2018; Haenseler et al., 2017; McQuade et al., 2018; Muffat et al., 2016; Pandya et al., 2017; Takata et al., 2017). While microglia as resident CNS immune cells are central players during neuroinflammatory insults, as mentioned above the involvement of infiltrating monocytes during neuroinflammation and degeneration should not be underestimated. It is therefore highly critical to investigate the action of potential neuro-immune modulators *in vitro* both on microglia and monocytes/macrophages and – maybe even more important – within a neural or neuro-inflammatory environment. In the present study we addressed this issue by performing a comparative immune polarisation experiments using murine iPSC-derived microglia, murine iPSC-derived macrophages and murine iPSC-derived macrophages cultured within a neural environment. Furthermore, observed differences in *in vitro* immune polarisation potential were validated *in vivo* following MCAO stroke and IL13-mediated therapeutic intervention thereon, thereby demonstrating that murine iPSC-derived microglia and iPSC-derived macrophage cell culture models are able to recapitulate several phenotypical properties of activated endogenous microglia and brain-infiltrating monocytes.

2. Methods

2.1. Mice

Wild-type (wt) C57BL/6 mice (strain code 027) were purchased from Charles River Laboratories. Transgenic C57BL/6-$CX_3CR1^{eGFP/eGFP}$ mice (strain code 005582) and $CCR2^{RFP/RFP}$ mice (strain code 017586) were purchased from Jackson Laboratories (JaxMice). $CX_3CR1^{eGFP/+}CCR2^{RFP/+}$ mice were obtained by breeding $CX_3CR1^{eGFP/eGFP}$ mice with $CCR2^{RFP/RFP}$ mice (Dooley et al., 2016; Hamzei Taj et al., 2018; Le Blon et al., 2016). During the entire study, mice were kept in the animalarium of the University of Antwerp (UA) or in the animal facility of the School of Medicine of the University of Barcelona under normal day-night cycle (12/12) with free access to food and water. All animal experimental procedures were approved by the Ethics Committee for Animal Experiments of the UA (approval no. 2015-84 and 2017-03) or by the Ethics Committee of the University of Barcelona (CEEA n° 367/17).

2.2. Generation of mitotically-inactivated mouse embryonic fibroblast (MEF) feeders

Immortalized MEFs (iMEFs) for support of iPSC cultures were kindly provided by Dr. Prim Singh (Nazarbayev University, Republic of Kazakhstan). iMEFs were cultured in standard cell culture flasks in DMEM supplemented with 10% (v/v) fetal bovine serum (FBS), 2 mM L-glutamine and 100 U/mL–100 µg/mL penicillin-streptomycin. iMEFs were split 1:3 every 3–4 days following cell detachment with a 0.05%

Trypsin-EDTA solution. To generate mitotically-inactivated feeders, iMEFs were harvested, γ-irradiated with 3000 rad in an XRAD320 irradiation device (Precision X-ray) and cryopreserved in FBS supplemented with 10% (v/v) DMSO (Sigma). Unless otherwise stated, here and below, all media and cell culture supplements were purchased from Thermo Fisher Scientific. Similarly, unless otherwise stated, all cell cultures, here and below, were maintained at 37 °C in a standard humidified cell culture incubator with 5% CO_2 (Thermo Fisher Scientific).

2.3. iPSC generation and culture

Murine iPSCs were generated from primary MEFs isolated from E14 embryos obtained from $CX_3CR1^{eGFP/eGFP} \times CCR2^{RFP/RFP}$ transgenic C57BL/6 mice. MEF isolation and reprogramming using pMX retroviral vectors encoding OCT4, SOX2 and KLF4 were performed as previously described (Pasque et al., 2014; Praet et al., 2014). Reprogramming experiments were performed using male MEFs. Embryonic stem cell (ESC)-like colonies were picked at day 16 of reprogramming and clonally expanded on mitotically-inactivated iMEFs in murine iPSC medium consisting of KnockOut DMEM supplemented with 15% (v/v) FBS, 1.5×10^6 U/mL leukaemia inhibiting factor (LIF; Millipore), 2 mM L-glutamine, 0.05 mM β-mercapto-ethanol, 1× nonessential amino acids (NEAA), 100 U/mL–100 μg/mL penicillin-streptomycin. The obtained iPSC lines were further named as $CX_3CR1^{eGFP/+}CCR2^{RFP/+}$ iPSCs. iPSC cultures were split 1:15 every other day following cell detachment with a 0.05% Trypsin-EDTA solution.

2.4. CX_3CR1-CCR2 genotyping

Genotyping of C57BL/6 wt, $CX_3CR1^{eGFP/eGFP}$ and $CCR2^{RFP/RFP}$ mice, as well as obtained $CX_3CR1^{eGFP/+}CCR2^{RFP/+}$ MEFs and $CX_3CR1^{eGFP/+}CCR2^{RFP/+}$ iPSCs was performed using primer sets and PCR conditions described by Jackson Laboratories for $CX_3CR1^{eGFP/eGFP}$ and $CCR2^{RFP/RFP}$ mice. PCR products were visualized on a 1.8% agarose gel using a Chemi-Doc MP Imaging System (Bio-Rad). Lengths of amplicons were compared to a TrackIt 1 kb DNA ladder (Thermo Fisher Scientific).

2.5. Isolation, culture and genetic engineering of embryonic brain-derived neural stem cell (NSC)

Adherently growing NSC cultures were obtained from E15 embryonic brains of wt C57BL/6 embryos (male and female) and cultured as previously described (Luyckx et al., 2018; Reekmans et al., 2011). NSC cultures were split 1:5 every 7 days following cell detachment using an Accutase solution (Sigma). In some experiments, for microscopic imaging of NSC co-cultures with iPSC-microglia, NSCs were transduced with a previously reported *pCHMWS-BFP-IRES-Pac* lentiviral vector (LVv) encoding the blue fluorescent protein (BFP) and the puromycin resistance protein (Guglielmetti et al., 2016; Reekmans et al., 2011), according to a previously optimized procedure for NSC transduction and puromycin selection (Reekmans et al., 2011). Following LVv transduction, BFP-expressing NSCs were selected using 1 μg/mL puromycin (InvivoGen). The resulting engineered NSC line was further named as BFP-NSC.

2.6. Production of L929-derived and bEnd5-derived conditioned medium (CM)

L929 cells (a murine fibrosarcoma cell line, ATCC CCL-1) were cultured in DMEM supplemented with 10% (v/v) FBS, 2 mM L-glutamine and 100 U/mL–100 μg/mL penicillin-streptomycin. bEnd5 cells (a murine endothelial cell line, ECACC 96091930) were cultured in DMEM supplemented with 10% (v/v) FBS, 2 mM L-glutamine, 1 mM Sodium Pyruvate, 0.05 mM β-mercapto-ethanol, 1× NEAA and 100 U/mL–100 μg/mL penicillin–streptomycin. L929 and bEnd5 cells were split 1:5 every 3–4 days following cell detachment with a 0.05% Trypsin-EDTA solution. For preparation of CM, L929 and bEnd5 cells were grown to confluence in T175 flasks in 25 ml of culture medium. Upon confluence 15 ml of culture medium was added and after 3 days the entire volume of medium was collected, filtered through a 0.22 μm membrane to remove cell debris and stored at −20 °C until further use.

2.7. Generation of iPSC-microglia

$CX_3CR1^{eGFP/+}CCR2^{RFP/+}$ iPSCs were seeded on agarose-coated (10 mg/ml in H_2O, 30 min at room temperature + 1 h at 37 °C) cell culture plates at a concentration of 10.000 cells/cm^2 to promote embryoid body (EB) formation in GMEM (Sigma) supplemented with 10% (v/v) FBS, 2 mM L-glutamine, 1 mM Sodium Pyruvate, 0.05 mM β-mercapto-ethanol, 1× NEAA and 100 U/mL–100 μg/mL penicillin-streptomycin, further referred as essential differentiation medium (EDM). On day 4, EBs were collected and transferred to a new agarose-coated cell culture plate in EDM. On day 8, EBs were seeded on gelatin-coated (0.01% in H_2O, 30 min at room temperature, Sigma) cell culture plates in fresh EDM supplemented with 100 ng/mL murine stem cell factor (SCF; ImmunoTools) and 5 ng/mL murine vascular endothelial growth factor-A (VEGF-A; ImmunoTools). On day 11, medium was changed to EDM supplemented with 1 ng/mL murine interleukin 3 (IL3; ImmunoTools), 20 ng/mL murine granulocyte-macrophage colony-stimulating factor (GM-CSF; ImmunoTools), 15% (v/v) L929-derived CM and 20% (v/v) bEnd5-derived CM. From differentiation day 15 on, a population of floating cells becomes spontaneously released in the supernatant of the culture, and from this point onward cultures were maintained in EDM until day 40 of differentiation. Between day 15 and day 40 of differentiation, floating cells were collected 2 times per week and further cultured on a confluent layer of NSCs or BFP-NSCs in EDM for 7 days, with medium change after 3–4 days. The cell population obtained was named iPSC-microglia. From this moment on, NSC + iPSC-microglia co-cultures were either directly used for stimulation experiments and/or immunocytochemistry analysis, or alternatively cells were harvested following cell detachment with a 0.05% Trypsin-EDTA solution and used for flow cytometric analysis or organotypic brain slice cultures (OBSCs) replenishment experiments.

2.8. Generation of iPSC-macrophages

iPSC-macrophages were differentiated from $CX_3CR1^{eGFP/+}CCR2^{RFP/+}$ iPSCs according to a previously published macrophage differentiation protocol for murine ESC (Zhuang et al., 2012), with minor modifications. Briefly, $CX_3CR1^{eGFP/+}CCR2^{RFP/+}$ iPSCs were seeded on agarose-coated cell culture plates at 10.000 cells/cm^2 to promote EB formation in macrophage differentiation medium (MDM) consisting of GMEM supplemented with 10% (v/v) FBS, 15% (v/v) L929-derived CM, 1 ng/mL IL3, 2 mM L-glutamine, 1 mM Sodium Pyruvate, 0.05 mM β-mercapto-ethanol, 1× NEAA and 100 U/mL–100 μg/mL penicillin-streptomycin. EBs were transferred to a new agarose-coated plate on day 4 and on day 6 in MDM. On day 8, EBs were seeded on gelatin-coated culture plates in MDM supplemented with 20 ng/mL GM-CSF. Between differentiation day 12 and day 30, floating macrophage precursors were collected, seeded on uncoated cell culture plates and further cultured in macrophage culture medium (MCM) consisting of GMEM supplemented with 10% (v/v) FBS, 15% (v/v) L929-derived CM, 20 ng/mL GM-CSF, 2 mM L-glutamine, 1× Sodium Pyruvate, 0.05 mM β-mercapto-ethanol, 1× NEAA and 100 U/mL–100 μg/mL penicillin-streptomycin. The resulting adherently growing cells were further named iPSC-macrophages. MCM was refreshed every 2–3 days and cells were split 1:5 every 5 days following cell detachment using a 0.05% Trypsin-EDTA solution. In a separate experiment (as indicated in the result Section 3.3), iPSC-macrophages were co-cultured for 7 days with NSCs in EDM in order to equal culture conditions described above for NSC + iPSC-microglia co-cultures.

2.9. Organotypic brain slice cultures (OBSCs)

OBSCs were prepared from wt C57BL/6 mice (male and female) according to the interphase method as previously described (Masuch et al., 2016; Stoppini et al., 1991; Vinet et al., 2012). In order to deplete OBSCs from endogenous microglia, OBSC medium was supplemented with 100 mg/ml clodronate disodium salt (Sigma) during the first 24 h of culture, after which medium was changed to OBSC medium. Microglia-depleted OBSCs were replenished with iPSC-microglia or iPSC-macrophages on day 7 of culture. For this, iPSC-microglia and iPSC-macrophages were harvested, washed and resuspended in OBSC medium, after which 0.5–1 × 10^5 cells were added in one drop (5–10 µL) directly onto the OBSCs. After replenishment, OBSCs were maintained in culture for 12 days before proceeding to microscopic analysis. Control non-depleted OBSCs, as well as control non-replenished microglia-depleted OBSCs, were equally cultured for a total of 20 days.

2.10. Flow cytometric analysis

The expression of CX_3CR1 (eGFP) and/or CCR2 (RFP) by $CX_3CR1^{eGFP/+}CCR2^{RFP/+}$ iPSC, iPSC-microglia progenitors (floating cell population), iPSC-microglia (in co-culture with NSCs) and iPSC-macrophages (in monoculture and in co-culture with NSCs) was assessed by direct detection of eGFP and/or RFP expression, respectively, by means of flow cytometry. For analysis of iPSC and iPSC-microglia progenitors, harvested cultures were directly stained with GelRed (10×, Biotium) in order to exclude dead cells from the analysis, and analysed using an Epics XL-MCL analytical flow cytometer (Beckman Coulter), according to previously established protocols (Costa et al., 2015; Reekmans et al., 2013). Data were analysed using FlowJo software (LLC) and reported as the percentage of $eGFP^+$ cells within the total viable cell population. For analysis of iPSC-microglia + NSC co-cultures, iPSC-macrophage monocultures and iPSC-macrophage + NSC co-cultures, harvested cells were co-stained with a phycoerythrin (PE)-Cy7-labelled anti-mouse CD45 antibody (0.8 µg/mL, Thermo Fisher Scientific, 25-0453-81) and a LIVE/DEAD™ Fixable Aqua Dead Cell Stain (Thermo Fisher Scientific), and analysed using a FACSAria II cell sorter (BD Biosciences), or co-stained with a phycoerythrin (PE)-labelled anti-mouse CD45 antibody (10 µg/mL, Thermo Fisher Scientific, 12-0451-82) and GelRed, and analysed using a Epics XL-MCL analytical flow cytometer according to previously optimized procedures (Hoornaert et al., 2016). Data were analysed using FacsDiva (BD Biosciences) or FlowJo software and reported as the percentage of $eGFP^+$ cells within the hematopoietic $CD45^+$ cell population.

2.11. Quantitative real time PCR (qRT-PCR)

Prior to RNA extraction, iPSC-microglia were isolated from iPSC-microglia + NSC co-cultures by positive immunoselection using the MACS CD45 Cell Isolation Kit (Miltenyi Biotec) according to the manufacturer's instructions. Total RNA was extracted from isolated iPSC-microglia, cultured iPSC-macrophages and undifferentiated $CX_3CR1^{eGFP/+}$ $CCR2^{RFP/+}$ iPSC using the RNAeasy Plus Mini Kit (Qiagen) according to the manufacturer's protocol. Total RNA (400 ng) was reverse-transcribed using the Omniscript RT kit (Qiagen). RT-qPCR was performed using the Power SYBR Green PCR Master Mix (Applied Biosystems) and the StepOnePlus Real-Time PCR System (Thermo Fisher Scientific). Thermal cycling conditions were 10 min at 95 °C and 40 cycles of 15 s at 95 °C and 1 min at 60 °C. Melt curves were performed upon completion of the cycles to ensure specificity of the product amplification. Primers were purchased from IDT. The following primer sequences were used: P2RY12-FOR 5′-CATTGACCGCTACCTGAAGACC-3′, P2RY12-REV 5′-GCCTCCTGTTGGTGAGAATCATG-3′ (Origene, MP212229); TMEM119-FOR 5′-GTGTCTAACAGGCCCCAGAA-3′, TMEM119-REV 5′-AGCCACGTGGTATCAAGGAG-3′ (Bennett et al., 2016); S100A4-FOR 5′-AGGAGCTACTGACCAGGGAG-3′, S100A4-REV 5′–CCTGTTGCTGTCCAAGTTGC-3′ (Hoeffel et al., 2015); GAPDH-FOR 5′-GGGGTCGTTGATGGCAACA-3′, GAPDH-REV 5′-AGGTCGGTGTGAACGGATTTG-3′ (Shu et al., 2017). The expression levels of P2RY12, TMEM119 and S100A4 mRNAs were normalized to GAPDH expression. Data were analysed with the 2-ΔΔCt method. Expression level of the genes of interest by iPSC-microglia (n = 4) and iPSC-macrophages (n = 4) are expressed as log2 fold versus expression level by undifferentiated $CX_3CR1^{eGFP/+}$ $CCR2^{RFP/+}$ iPSC (n = 3).

2.12. Bone marrow (BM) and brain cell isolation and flow cytometric analysis

For BM cell isolation, 10–14 weeks old $CX_3CR1^{eGFP/+}$ $CCR2^{RFP/+}$ male mice were used. Mice were euthanized, the femurs and tibias from the hind limbs were extracted and flushed with Hank's balanced salt solution without calcium and magnesium (HBSS-Ca^{2+}/Mg^{2+}) supplemented with 10% (v/v) FBS. Cells were filtered using a 40 µm nylon cell strainer (BD Biosciences), centrifuged at 300*g* for 10 min at 4 °C and resuspended in 3 ml of red blood cell lysis buffer (ACK; 155 mM NH_4Cl, 10 mM $KHCO_3$, 0.1 mM EDTA, pH 7.3) for 5 min at room temperature. Cells were extensively washed with 40 ml of PBS, 2 mM EDTA, 2% (v/v) FBS (FACS buffer) and centrifuged again at 300*g* for 10 min at 4 °C. For flow cytometric analysis BM cells were diluted 1:1 with FACS buffer supplemented with 5 mg/ml Fcblock (clone 2.4G2, BD) incubated 10 min at 4 °C and analysed for the expression of CX_3CR1 (eGFP) and CCR2 (RFP) using a BD LSRII cytometer (BD Biosciences).

For brain cell isolation, 12–14 weeks old $CX_3CR1^{eGFP/+}$ $CCR2^{RFP/+}$ male mice were used. Cell isolation from brain tissue was performed as described (Pedragosa et al., 2018). For flow cytometric analysis brain cells were co-stained with a BV786-labelled anti-mouse CD45 antibody (0.2 mg/ml, BD Bioscience, 564225) and a APC-Cy7-labelled anti-mouse CD11b antibody (0.2 mg/ml, BD Bioscience, 557657) and analyzed for the expression of CX_3CR1 (eGFP), CCR2 (RFP), CD45 and CD11b using a BD LSRII cytometer (BD Biosciences). Data were analysed using FlowJo software.

2.13. In vitro stimulation experiments

NSC cultures (in NEM), iPSC-microglia + NSC co-cultures (in EDM), iPSC-macrophage monocultures (in MCM) and iPSC-macrophage + NSC co-cultures (in EDM) were prepared on coverslips in 24-well plates in 1 ml of culture medium. Pro-inflammatory stimulation experiments were performed using 1 µg/mL lipopolysaccharide (LPS; Sigma) and 50 ng/mL interferon γ (IFNγ; ImmunoTools). After 24 h of stimulation, supernatants were harvested from non-stimulated and stimulated cultures and analysed in triplicate for the presence of tumour necrosis factor alpha (TNFα), interleukin 6 (IL6) and interleukin 10 (IL10) using ELISA kits (BioLegend), according to the manufacturer's instructions. Alternative activation experiments were performed using 100 ng/mL IL13 (ImmunoTools) for 48 h. All cultures were processed for further immunocytochemistry analyses.

2.14. Experimental stroke and cell transplantation in mice

Ischemic stroke was induced in 10 male $CX_3CR1^{eGFP/+}CCR2^{RFP/+}$ mice (11–13 weeks, 22–26 g) by middle cerebral artery occlusion (MCAO) technique. Two days after induction of ischemic stroke, 5 mice randomly selected received an intracerebral transplantation of IL13-producing mesenchymal stem cells (MSCs) as previously reported (Hamzei Taj et al., 2018). MCAO mice were perfusion-fixed (4% w/v paraformaldehyde, PFA, Sigma) at day 14 after stroke induction and dissected brains were processed for cryo-sectioning, as previously reported (Hamzei Taj et al., 2018).

2.15. Immunofluorescence stainings

For immunostaining of cultured cells (iPSCs, iPSC-microglia + NSC co-cultures, iPSC-macrophages, and iPSC-macrophage + NSC co-cultures; control and following LPS + IFNγ or IL13 stimulation), cell cultures (prepared on glass coverslips) were fixed with 4% (w/v) PFA for 20 min at 4 °C. For immunostaining of OBSCs (control, microglia-depleted and replenished with iPSC-microglia or iPSC-macrophages), OBSCs were fixed with 4% (w/v) PFA for 3.5 h at 4 °C. For immunostaining of brain tissue sections (MCAO and MCAO + IL13-MSC transplant), 10 µm cryo-sections on poly-L-lysine (PLL, Sigma)-coated glass slides were used. For all immunostainings similar procedures were used, according to previously optimised protocols (Hamzei Taj et al., 2018; Praet et al., 2014; Reekmans et al., 2013). Briefly, coverslips or slides were rinsed in tris buffered saline (TBS) and incubated first with a permeabilization solution consisting of Triton-X-100 (0.1% (v/v) in TBS, Sigma) for 30 min at room temperature, then with a blocking solution consisting of TBS supplemented with 20% (v/v) blocking serum (from the same host species as the secondary antibody, Jackson ImmunoResearch) for 1 h at room temperature. OBSCs were incubated with a permeabilization and blocking solution consisting of TBS supplemented with 20% (v/v) blocking serum and 0.3% (v/v) Triton-X-100 for 3 h at room temperature. Subsequently, samples were incubated with the primary antibody (or antibodies) in milk solution (10% (w/v) in TBS, Sigma) for coverslips and slides or TBS supplemented with 1% (v/v) blocking serum and 0.3% (v/v) Triton-X-100 for OBSCs, i.e. staining buffer, overnight at 4 °C. Next, samples were rinsed in TBS and incubated with the secondary antibody (or antibodies) in staining buffer at room temperature (1 h for coverslips and slides, 2 h for OBSCs). Nuclear staining was performed using 1 µg/mL DAPI (Thermo Fisher Scientific) or 5 µM TOPRO-3 (Thermo Fisher Scientific) solutions (both in TBS). Next, stained coverslips, OBSCs and slides were mounted with Prolong Gold antifade reagent (Thermo Fisher Scientific) and images were acquired at room temperature using an Olympus BX51 fluorescence microscope equipped with an Olympus DP71 digital camera. The following objective lenses were employed: UPlanFL-N 20×/0.5, UPlanFL-N 40×/0.75 and UPlanFL-N 100×/1.3 (Olympus). Olympus CellSens software was used for image acquisition and processing. For immunostainings, the following antibody combinations were used: a goat anti-mouse DPPA4 antibody (0.4 µg/mL, R&D Systems, AF3730) in combination with an Alexa Fluor 555-labelled donkey anti-goat secondary antibody (10 µg/mL, Thermo Fisher Scientific, A21432), a rabbit anti-mouse Iba-1 antibody (2 µg/mL, Wako, 019-19741) in combination with an Alexa Fluor 555-labelled donkey anti-rabbit secondary antibody (2 µg/mL, Thermo Fisher Scientific, A31572), a goat anti-mouse eGFP antibody (2 µg/mL, Abcam, ab6673) in combination with a Cy5-labelled donkey anti-goat secondary antibody (10 µg/mL, Abcam, ab6566), a rat anti-mouse F4/80 antibody (4 µg/mL, AbD Serotec, 019–19741) in combination with an Alexa Fluor 555-labelled goat anti-rat secondary antibody (2 µg/mL, Thermo Fisher Scientific, A21434) or an Alexa Fluor 350-labelled donkey anti-rat secondary antibody (10 µg/mL, Thermo Fisher Scientific, A21093), a biotinylated rat anti-mouse MHC-II antibody (2.5 µg/mL, Thermo Fisher Scientific) in combination with Cy5-labelled streptavidin (20 µg/mL, Thermo Fisher Scientific, SA1011), a rat anti-mouse MHC-II antibody (2,5µg/ml, Thermo Fisher Scientific, 14-5321-82) in combination with an Alexa Fluor 350-labelled goat anti-rat secondary antibody (10 µg/mL, Thermo Fisher Scientific, A21093), a rabbit anti-mouse RFP antibody (2.5 µg/mL, Abcam, ab62341) in combination with an Alexa Fluor 555-labelled donkey anti-rabbit secondary antibody (2 µg/mL, Thermo Fisher Scientific, A31572), a mouse anti-mouse Arginase-1 antibody (1 µg/mL, Santa Cruz Biotechnology, sc271430) in combination with an Alexa Fluor 555-labelled goat anti-mouse secondary antibody (10 µg/mL, Thermo Fisher Scientific, A21127), a goat anti-mouse Arginase-1 antibody (4 µg/mL, Santa Cruz, sc18354) in combination with a donkey anti-goat Alexa Fluor 350-labelled secondary antibody (10 µg/mL, Thermo Fisher Scientific, A21081), a rabbit anti-mouse Ym1 antibody (2.5 µg/mL, Stemcell technologies, 01404) in combination with an Alexa Fluor 555-labelled donkey anti-rabbit secondary antibody (2 µg/mL, Thermo Fisher Scientific, A31572) or an Alexa Fluor 350-labelled donkey anti-rabbit secondary antibody (10 µg/mL, Thermo Fisher Scientific, A10039), phycoerythrin (PE)-labelled anti-mouse CD45 antibody (10 µg/mL, Thermo Fisher Scientific, 12-0451-82).

2.16. Quantification of immunofluorescence stainings

Quantitative analyses of immunofluorescence data were performed using TissueQuest (TissueGnostics) immunofluorescence analysis software as previously described (Hamzei Taj et al., 2018; Praet et al., 2014). For the analysis of MCAO-stroke lesions in $CX_3CR1^{eGFP/+}CCR2^{RFP/+}$ reporter gene transgenic mice, one slide per brain was analysed. Per slide, one picture covering a cortical lesion and corresponding contralateral picture were taken at 20× magnification. For each picture, one representative region of interest (ROI) was manually selected for further analysis. For the analysis of *in vitro* iPSC-microglia and iPSC-macrophage cultures, multiple coverslips per condition were analysed, whereby pictures were taken at 20× or 40× magnification at randomly selected ROIs. Cellular recognition was performed based on nuclear staining (nuclei size, staining intensity and discrimination by area were optimized manually), followed by the analysis of specific staining. To discriminate false signals the cut-off was defined for each quantified image. Scattergrams were generated to visualize the corresponding positive cells in the source image and the relative number of cells expressing the markers F4/80, MHC-II, Ym1 and Arginase-1 were obtained. F4/80 mean intensity values were analysed within the $F4/80^+$ population.

2.17. Statistical analysis

Differential gene expression measured by qRT-PCR (Fig. 1) was analysed with a linear mixed-model in JMP Pro 14 (SAS) to account for repeated measures for each independent sample. The linear mixed-model analysis was fitted for each gene separately using log2 fold change of expression as dependent variable, cell type as fixed effect and single sample as random effect. Multiple comparison correction was performed with the Tukey-HSD test. Significant differences between iPSC-microglia and iPSC macrophages were reported. Comparison of average number of $IBA1^+$ cells in OBSC brain slices between control and clodronate treatment (Fig. 1) were analysed using the Generalized Estimating Equations (GEE) model (Zeger et al., 1988) to take into account repeated measures for each observation. Differences in the percentage of $eGFP^+$ cells and in the median fluorescence intensity of the eGFP signal between cell types (Fig. 3) were analysed by Mann–Whitney U tests in GraphPad Prism 6.0. For the quantitative immunofluorescence data the following techniques were applied: (i) Comparison of mean difference in F480 MFI between control and LPS + IFNγ stimulation for each cell type and among cell types (Fig. 4) was analysed using GEE. Since the data originated from 2 independent experiments, the GEE model was corrected for potential differences in experiments for those groups present in both experiments. The additional variable indicated the incremental effect of F480 MFI in experiment 2 compared to experiment 1, for each group present in both experiments. The necessity of these terms was tested for using a Wald test. If a statistically significant incremental effect of experiment 2 compared to experiment 1 was present, linear combinations were used to summarize the effect of the treatment and to make pairwise comparisons. (ii) Comparison of difference in MHC-II% between control and LPS + IFNγ stimulation for cell type and differences in MHC-II% between cell types (Fig. 4) were analyzed using GEE. Due to separation issues, a 1 was added to the numerator and denominator and the remainder of this analysis was performed as described in (i). (iii) The proportion of $F4/80^+$ cells and $MHC\text{-}II^+$ cells in the cortex region of

the MCAO lesion side between microglia and monocytes (Fig. 4) was compared using GEE. (iv) Comparison of mean Ym1 and Arginase-1 expression between cell types was only performed for IL13-stimulated samples (Fig. 5). Since the results originated from 3 independent experiments, an additional factor was included in the GEE model to account for potential differences between experiments. (v) The proportion of $Ym1^+$ cells and $Arginase\text{-}1^+$ cells in the cortex region of the MCAO lesion transplanted with IL13-MSC was compared between CX_3CR1^+ cells and $CCR2^+$ monocytes (Fig. 5) using GEE. Comparison of mean TNFα and IL6 secretion was investigated in 4 independent experiments and mean IL10 secretion (Fig. 4) in 3 independent experiments using GEE. Since the data originated from either 4 or 3 independent experiments, the GEE model was corrected for potential differences in experiments. A GEE model without intercept was fitted with factors expressing the experiment-specific mean cytokine secretion for each cell type (iPSC-microglia + NSC, iPSC-macrophages and iPSC-macrophages + NSC) and treatment (control and LPS + IFNγ), resulting in either 15 or 11 factors. Linear combinations were used to summarize the effect of the cell type and treatment effect across experiments and to make pairwise comparisons. For all the analyses P-values were corrected for multiple testing using the false-discovery rate procedure (Benjamini and Hochberg, 1995). A p-value < 0.05 is considered as

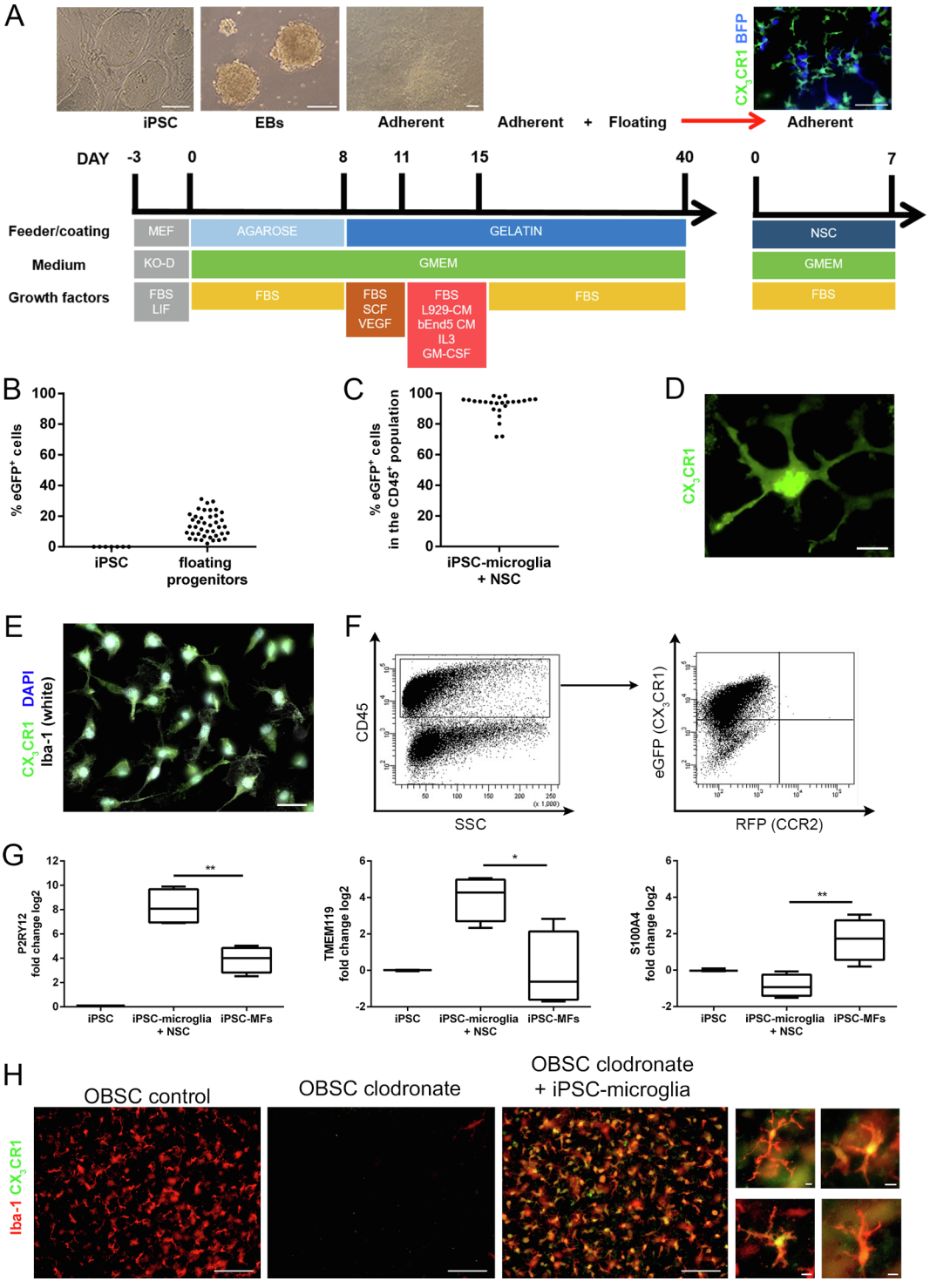

(caption on next page)

Fig. 1. In vitro differentiation of $CX_3CR1^+CCR2^-$ iPSC-microglia from murine $CX_3CR1^{eGFP/+}CCR2^{RFP/+}$ iPSCs. A) Schematic outline of the optimized iPSC-microglia differentiation protocol indicating the media, the growth factors and the feeder/coating employed during the different stages of differentiation. Representative images showing culture appearance during differentiation. From left to right: $CX_3CR1^{eGFP/+}CCR2^{RFP/+}$ iPSC colonies cultured on mitotically inactivated iMEFs, EBs formation, development of EB-derived adherent cultures on gelatin-coated plates, CX_3CR1^+ ($eGFP^+$) iPSC-microglia in co-culture with BFP-NSCs. The scale bars indicate 100 μm. B) Graph showing the percentage of cells expressing eGFP (CX_3CR1), measured by flow cytometry, in undifferentiated $CX_3CR1^{eGFP/+}CCR2^{RFP/+}$ iPSC cultures (n = 7) and in floating cells harvested between day 15–40 of differentiation (n = 40). C) Graph showing the percentage of cells expressing eGFP (CX_3CR1), measured by flow cytometry, within the $CD45^+$ population in co-cultures of iPSC-microglia + NSC (n = 24). D) Detailed image depicting the ramified morphology of CX_3CR1^+ ($eGFP^+$) iPSC-microglia. CX_3CR1 (eGFP) is directly visible as green fluorescence. The scale bar indicates 20 μm. E) Representative immunofluorescence image showing expression of the general microglia/macrophage marker Iba-1 by CX_3CR1^+ ($eGFP^+$) iPSC-microglia. The secondary antibody against Iba-1 was coupled to Alexa Fluor 555 (red fluorescence) but shown here in white, CX_3CR1 (eGFP) is directly visible as green fluorescence and nuclei are identified by DAPI staining (in blue). The scale bar indicates 20 μm. F) Representative flow cytometric analysis showing that iPSC-microglia cultures express CD45 (left plot) and CX_3CR1 (eGFP, right plot), but not CCR2 (RFP, right plot) (n = 7). G) Box plots showing mRNA expression of P2RY12, TMEM119 and S100A4 in undifferentiated $CX_3CR1^{eGFP/+}CCR2^{RFP/+}$ iPSC (n = 3), iPSC-microglia (n = 4) and iPSC-macrophages (n = 4) assessed by qRT-PCR and normalized to the mean expression value of the respective gene in undifferentiated $CX_3CR1^{eGFP/+}CCR2^{RFP/+}$ iPSC. Data are expressed as log2 fold change. Box plots indicate median and interquartile ranges, whiskers indicate the minimum and maximum values. *$p < 0.05$; **$p < 0.01$. H) Representative immunofluorescence images of non-depleted (control) OBSCs (n = 4), clodronate-treated (depleted of endogenous microglia) OBSCs (n = 3) and clodronate-treated OBSCs replenished with CX_3CR1^+ ($eGFP^+$) iPSC-microglia (n = 9) stained with an antibody for the general microglia/macrophage marker Iba-1. CX_3CR1^+ ($eGFP^+$) iPSC-microglia colonized microglia-depleted OBSCs and showed highly ramified morphology (higher magnification images). Secondary antibody for Iba-1 was coupled to Alexa Fluor 555 (red fluorescence), CX_3CR1 (eGFP) is directly visible as green fluorescence. The scale bars in the main images indicate 100 μm and in the higher magnification images 10 μm. Abbreviations: BFP, blue fluorescent protein; CM, conditioned medium; CCR2, C–C chemokine receptor 2; CX_3CR1, CX_3C chemokine receptor 1; EBs, embryoid bodies; eGFP, enhanced green fluorescent protein; FBS, fetal bovine serum; GM-CSF, granulocyte-macrophage colony-stimulating factor; Iba-1, ionized calcium-binding adapter molecule 1; IL3, interleukin 3; iPSC, induced pluripotent stem cell; LIF, leukemia inhibiting factor; MEF, mouse embryonic fibroblast; NSC, neural stem cell; OBSCs, organotypic brain slice cultures; P2RY12, Purinergic Receptor P2Y12; RFP, red fluorescent protein; S100A4, S100 Calcium Binding Protein A4; SCF, stem cell factor; SSC, side scatter; TMEM119, transmembrane protein 119; VEGF, vascular endothelial growth factor. (For interpretation of the references to colour in this figure legend, the reader is referred to the web version of this article.)

statistically significant. All statistical analyses were performed using the statistical software R version 3.5.0 (https://www.R-project.org/), unless otherwise stated.

3. Results

3.1. In vitro differentiation of $CX_3CR1^+CCR2^-$ iPSC-microglia from murine $CX_3CR1^{eGFP/+}CCR2^{RFP/+}$ iPSCs

Murine iPSCs were generated by retroviral reprograming of mouse embryonic fibroblast (MEFs) cultured from $CX_3CR1^{eGFP/eGFP}$ X $CCR2^{RFP/RFP}$mice and used as starting material for *in vitro* differentiation of iPSC-microglia. $CX_3CR1^{eGFP/+}CCR2^{RFP/+}$ iPSCs were characterized based on colony morphology (Fig. 1A), expression of the developmental pluripotency associated 4 (DPPA4) protein (Fig. S1A), absence of eGFP/RFP expression (Fig. S1B) and $CX_3CR1^{eGFP/+}CCR2^{RFP/+}$ genotype (Fig. S1C). A two-stage differentiation protocol based on existing literature (Brownjohn et al., 2018; Douvaras et al., 2017; Pandya et al., 2017), with minor modifications, was employed to generate murine iPSC-microglia. During the first stage of differentiation, $CX_3CR1^{eGFP/+}CCR2^{RFP/+}$ iPSCs were initially allowed to form EBs. Next, 8 days-old EBs were seeded on gelatin-coated plates to enable adherent cell growth and culture medium was

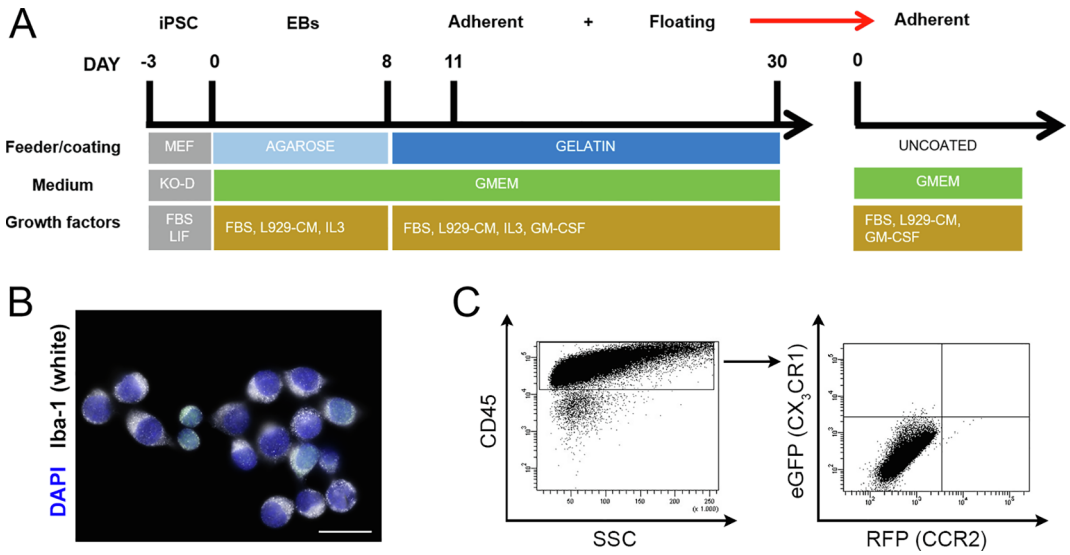

Fig. 2. In vitro differentiation of $CX_3CR1^-CCR2^-$ iPSC-macrophages from murine $CX_3CR1^{eGFP/+}CCR2^{RFP/+}$ iPSCs. A) Schematic outline of the iPSC-macrophage differentiation protocol indicating the media, the growth factors and the coating employed during the different stages of differentiation. B) Representative immunofluorescence image showing expression of the general microglia/macrophage marker Iba-1 by iPSC-macrophages. The secondary antibody against Iba-1 was coupled to Alexa Fluor 555 (red fluorescence) but shown here in white and nuclei are identified by DAPI staining (in blue). The scale bars indicate 20 μm. C) Flow cytometry plots showing that iPSC-macrophage cultures express CD45 (left plot), but no CX_3CR1 (eGFP) or CCR2 (RFP) (right plot) (n = 5). Abbreviations: CCR2, C–C chemokine receptor 2; CM, conditioned medium; CX_3CR1, CX_3C chemokine receptor 1; EBs, embryoid bodies; eGFP, enhanced green fluorescent protein; FBS, fetal bovine serum; GM-CSF, granulocyte-macrophage colony-stimulating factor; Iba-1, ionized calcium-binding adapter molecule 1; IL3, interleukin 3; iPSC, induced pluripotent stem cell; LIF, leukemia inhibiting factor; MEF, mouse embryonic fibroblast; RFP, red fluorescent protein; SSC, side scatter. (For interpretation of the references to colour in this figure legend, the reader is referred to the web version of this article.)

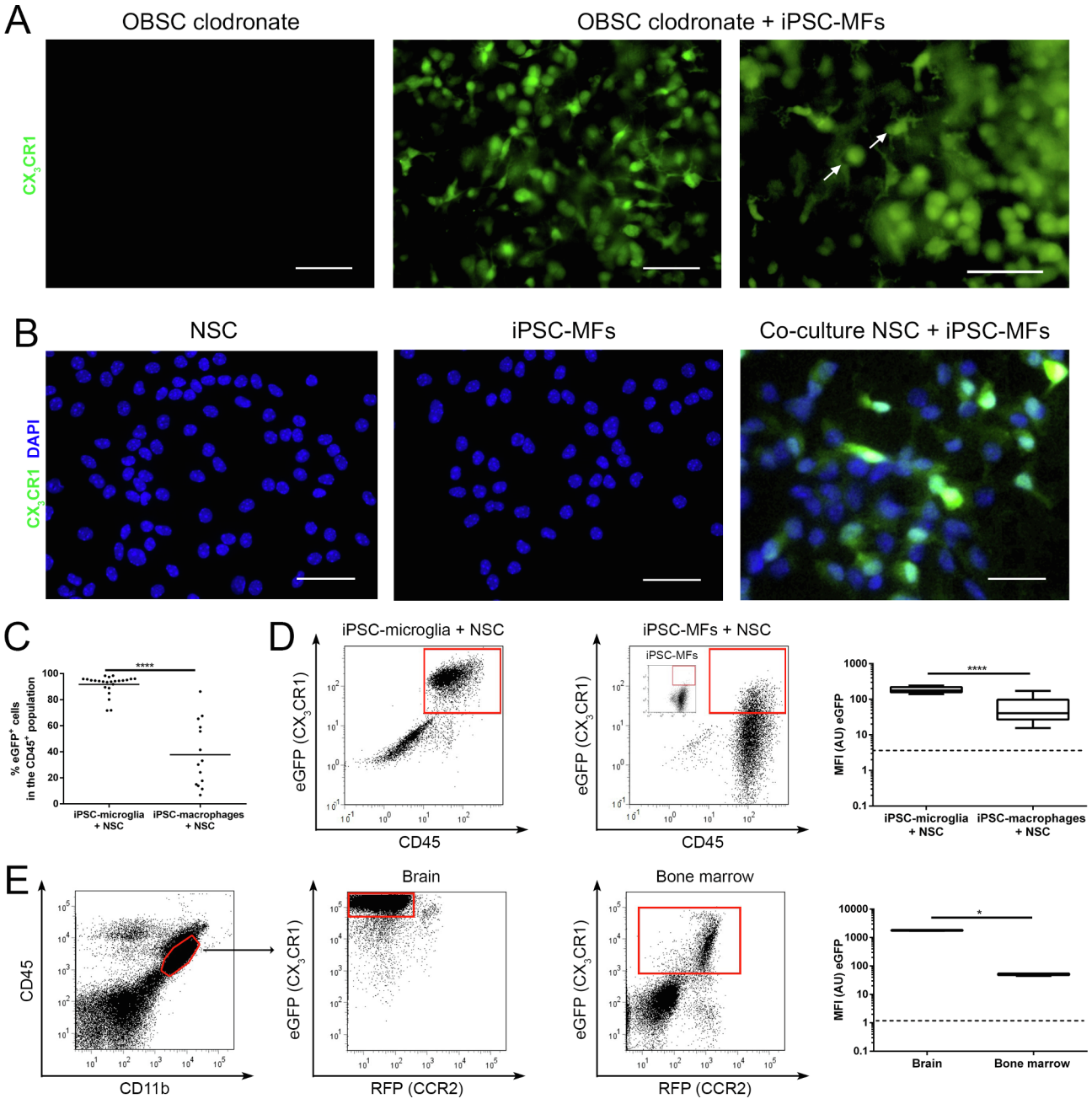

Fig. 3. $CX_3CR1^-CCR2^-$ iPSC-macrophages redefine their morphological and phenotypical properties following interaction with a neural environment. A) Representative immunofluorescence image of clodronate-treated OBSCs control (n = 3) and replenished with $CX_3CR1^-CCR2^-$ ($eGFP^-RFP^-$) iPSC-macrophages (n = 3) showing upregulation of CX_3CR1 on iPSC-macrophages (left image). Higher magnification image (right) depicting multiple morphological appearances of CX_3CR1^+ ($eGFP^+$) iPSC-macrophages within OBSC cultures. CX_3CR1 (eGFP) expression is directly visible as green fluorescence. The scale bars indicate 50 μm. (B) Representative image showing expression of CX_3CR1 (eGFP) by NSCs (n = 6), iPSC-macrophages (n = 12) and iPSC-macrophages co-cultured for 7 days with NSCs (n = 9). CX_3CR1 (eGFP) expression is directly visible as green fluorescence and nuclei are identified by DAPI staining (in blue). The scale bar indicates 50 μm. C) Graph showing the percentage of cells expressing eGFP (CX_3CR1), measured by flow cytometry, within the $CD45^+$ population in co-cultures of iPSC-microglia + NSC (n = 24) and iPSC-macrophages + NSC (n = 14). D) FACS plots depicting the gating strategy employed to select the eGFP (CX_3CR1)-expressing population within co-cultures of iPSC-microglia + NSC (n = 20) and iPSC-macrophages + NSC (n = 12). The inset displays the absence of eGFP (CX_3CR1)-expressing cells within the iPSC-macrophages monoculture. Graph showing the median fluorescence intensity (MFI) of the eGFP signal of these populations. The dotted line indicates the background fluorescence. E) FACS plots depicting the gating strategy employed to select the eGFP (CX_3CR1)-expressing microglia population isolated from brain tissue (n = 4) and the eGFP (CX_3CR1)-expressing macrophage population isolated from bone marrow (n = 5) from $CX_3CR1^{eGFP/+}$ $CCR2^{RFP/+}$ mice. Graph showing the MFI of the eGFP signal of these populations. The dotted line indicates the background fluorescence. Box plots indicate median and interquartile ranges, whiskers indicate the minimum and maximum values. *$p < 0.05$; ****$p < 0.0001$. Abbreviations: AU, arbitrary unit; CCR2, C–C chemokine receptor 2; CX_3CR1, CX_3C chemokine receptor 1; eGFP, enhanced green fluorescent protein; iPSC, induced pluripotent stem cell; MFs, macrophages; MFI, median fluorescence intensity; NSC, neural stem cell; OBSCs, organotypic brain slice cultures; RFP, red fluorescent protein. (For interpretation of the references to colour in this figure legend, the reader is referred to the web version of this article.)

supplemented for 3 days with SCF and VEGF, and subsequently for 4 days with IL3, GM-CSF and CM obtained from L-929 and bEnd5 cell lines to support myeloid progenitor differentiation and expansion (Fig. 1A). From day 15 onwards the differentiated culture continuously released in the supernatant a viable (66 ± 9% STD, n = 40) population of floating cells containing CX_3CR1^+ ($eGFP^+$) myeloid progenitors (Fig. 1B). In order to mimic the migration of CX_3CR1^+ myeloid progenitors to the embryonic brain, during the second stage of differentiation the floating fraction containing $eGFP^+$ cells was co-cultured for 7 days with embryonic brain-derived NSCs (Fig. 1A). Subsequently, a homogeneous population of ramified $eGFP^+$ (CX_3CR1^+) iPSC-microglia (Fig. 1A, C and D) was obtained. Murine CX_3CR1^+ iPSC-microglia displayed expression of the myeloid marker Iba-1

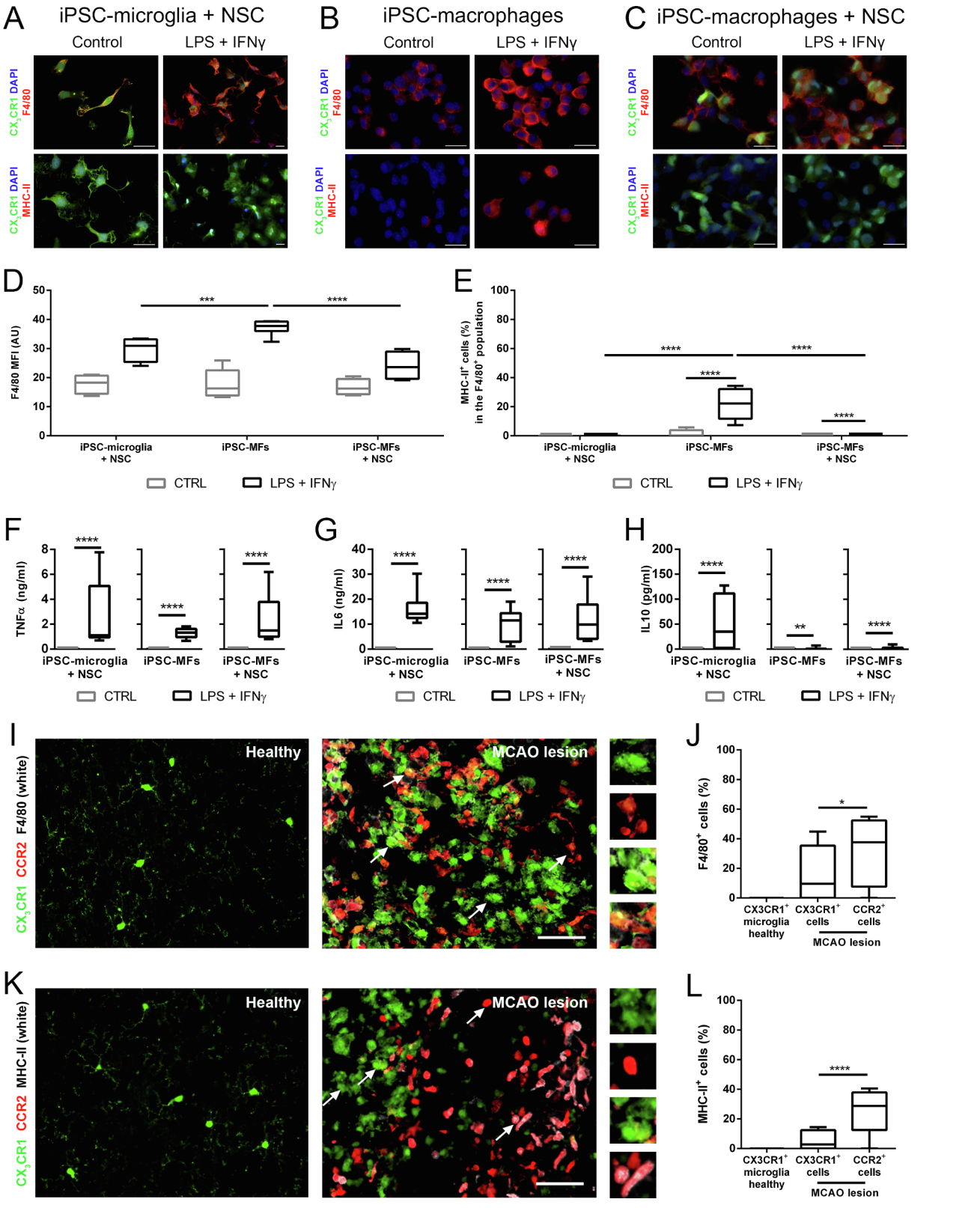

(caption on next page)

Fig. 4. Phenotypical properties of classically activated iPSC-microglia, iPSC-macrophages and NSC-primed iPSC-macrophages resemble the *in vivo* phenotypical profile of murine microglia and monocytes within stroke lesions. Representative immunofluorescence images showing the expression of the activation markers F4/80 and MHC-II on A) iPSC-microglia in co-culture with NSCs, B) iPSC-macrophage monocultures and C) NSC-primed iPSC-macrophages under baseline culture conditions (control) and following stimulation with LPS + IFNγ (activated). The secondary antibody against F4/80 was coupled to Alexa Fluor 555 (red fluorescence), the secondary antibody against MHC-II was coupled to Cy5 (far-red fluorescence) but shown here in red, CX_3CR1 (eGFP) is directly visible as green fluorescence and nuclei are identified by DAPI staining (in blue). The scale bars indicate 20 μm. Quantitative analysis of the immunofluorescence images was performed for n = 4 per condition for iPSC-microglia + NSC and iPSC-macrophages + NSC and n = 8 per condition for iPSC-macrophage monocultures. D) Box plots showing the level of F4/80 expression under control and activated conditions, expressed as mean fluorescence intensity (MFI). E) Box plots showing the percentage of cells expressing MHC-II within the $F4/80^+$ population under control and activated conditions. Cytokine production by iPSC-microglia, iPSC-macrophages and NSC-primed iPSC-macrophages under baseline culture conditions and following LPS + IFNγ stimulation. Box plots showing the amount of F) TNF-α, G) IL6 and H) IL10 produced by 100.000 cells during 24 h of culture in 2 or 3 independent experiments (n = 6 per condition). Representative immunofluorescence images showing the expression of the activation markers I) F4/80 and K) MHC-II in healthy brain tissue (left images) and a MCAO-induced brain lesion (right images) in $CX_3CR1^{eGFP/+}CCR2^{RFP/+}$ mice. White arrows indicate the illustrative close-up images (panel next to right image). The secondary antibodies against F4/80 and MHC-II were coupled to Alexa Fluor 350 (blue fluorescence) but shown here in white, the secondary antibody against RFP (associated with CCR2 expression) was coupled to Alexa Fluor 555 (red fluorescence) and CX_3CR1 (eGFP) expression is directly visible as green fluorescence. The scale bars indicate 100 μm. Quantitative analysis of the immunofluorescence images was performed on brain slices obtained from 5 mice. Box-plots showing the percentage of J) F4/80 and L) MHC-II expression by CX_3CR1^+ microglia in healthy brain tissue (contralateral), and CX_3CR1^+ cells and $CCR2^+$ monocytes within a MCAO-induced stroke lesion. Box plots indicate median and interquartile range, whiskers indicate the minimum and maximum values. *p < 0.05; ***p < 0.001; ****p < 0.0001. Abbreviations: AU, arbitrary unit; CCR2, C–C chemokine receptor type 2; CX_3CR1, CX_3C chemokine receptor 1; CTRL, control; IFN-γ, interferon γ; IL6, interleukin 6; IL10, interleukin 10; iPSC, induced pluripotent stem cell; LPS Lipopolysaccharides; MCAO, middle cerebral arterial occlusion; MFs, macrophages; MFI, mean fluorescence intensity; MHC, major histocompatibility complex; NSC, neural stem cell; TNFα, tumor necrosis factor. (For interpretation of the references to colour in this figure legend, the reader is referred to the web version of this article.)

(Fig. 1E) and absence of the chemokine receptor CCR2 (RFP) (Fig. 1F). Furthermore, comparative qRT-PCR experiments highlighted that iPSC-microglia expressed significantly higher levels of mRNA for the microglia-specific proteins P2RY12 and TMEM119 as compared to iPSC-macrophages, whereas mRNA for the macrophage-associated migration molecule S100A4 was significantly lower (or not) expressed by iPSC-microglia as compared to iPSC-macrophages (Fig. 1G). We further investigated the ability of iPSC-microglia to *ex vivo* engraft brain tissue using OBSCs. For this, wild type OBSCs (Fig. 1H, left side) were depleted from endogenous microglia by clodronate treatment (Fig. 1H, centre; significant reduction in the number of $Iba\text{-}1^+$ cells as compared to control OBSCs; 88%, p < 0.0001) and seeded with CX_3CR1^+ iPSC-microglia. After two weeks of culture, Iba-1 immunostaining combined with direct eGFP fluorescence (Fig. 1H, right side) revealed that CX_3CR1^+ iPSC-microglia efficiently colonized microglia-depleted OBSCs and obtained the typical highly ramified microglia morphology.

3.2. *In vitro differentiation of $CX_3CR1^-CCR2^-$ iPSC-macrophages from murine $CX_3CR1^{eGFP/+}CCR2^{RFP/+}$ iPSCs*

In order to differentiate $CX_3CR1^{eGFP/+}CCR2^{RFP/+}$ iPSCs into macrophages we applied an optimized culture protocol for the production of murine embryonic stem cell-derived macrophages (Zhuang et al., 2012), with minor modifications (Fig. 2A). At first, $CX_3CR1^{eGFP/+}CCR2^{RFP/+}$ iPSCs were differentiated into EBs in culture medium supplemented with IL3 and CM obtained from L-929 cells to promote immediate commitment towards the myeloid lineage. Next, 8 days-old EBs were transferred to gelatin-coated plates and cultured using the differentiation medium described above additionally supplemented with GM-CSF. Over the next 3 days, non-adherent macrophage precursors were released into the culture supernatant. The floating population was then further cultured on uncoated plates in medium supplemented with GM-CSF and CM obtained from L-929 cells to achieve terminal differentiation. Obtained iPSC-macrophages were round-shaped and displayed homogeneous expression of Iba-1 (Fig. 2B). Flow cytometric analysis demonstrated absence of the chemokine receptors CCR2 and CX_3CR1 (Fig. 2C). Finally, as already described in Section 3.1, iPSC-macrophages expressed a significantly higher mRNA level for the macrophage-specific protein S100A4 as compared to iPSC-microglia, while expression of mRNA encoding the microglia-specific proteins P2RY12 and TMEM119 was highly reduced (or absent) in iPSC-macrophages as compared to iPSC-microglia (Fig. 1G).

3.3. *Murine iPSC-macrophages acquire microglial characteristics upon interaction with a neural environment*

Given the complexity of neuroinflammatory lesions, whereby infiltrating monocytes co-orchestrate the neuropathological environment, we here evaluated whether CX_3CR1^- ($eGFP^-$) iPSC-macrophages were able to respond to brain-specific signalling and to what extent the culture environment could influence their phenotypical properties. As shown in Fig. 3A, CX_3CR1^- ($eGFP^-$) iPSC-macrophages partially upregulated CX_3CR1 (eGFP) expression when seeded on microglia-depleted OBSCs. However, while iPSC-microglia on OBSCs nearly all acquired the typical microglia ramification (Fig. 1H), iPSC-macrophages on OBSCs displayed multiple appearances, ranging from round-shaped morphology to some degree of microglia-like ramification (Fig. 3A). Similarly, a subset of iPSC-macrophages co-cultured for 7 days with NSCs partially upregulated CX_3CR1 (eGFP) expression (Fig. 3B), although the number of NSC-primed iPSC-macrophages expressing eGFP was significantly lower as compared to iPSC-microglia (Fig. 3C, p < 0.0001). We here also observed that the median fluorescence intensity (MFI) of eGFP (CX_3CR1) expression was significantly different for iPSC-microglia as compared to NSC-primed iPSC-macrophages (Fig. 3D, p < 0.0001). For comparison, we analysed by flow cytometry the level of eGFP expression by brain-resident microglia and bone marrow (BM) macrophages in $CX_3CR1^{eGFP/+}CCR2^{RFP/+}$ mice and demonstrate – in agreement with the above described data – that the level of eGFP expression by a subpopulation of BM macrophages was notably different as compared to brain-resident microglia (Fig. 3E, p = 0.0159). Finally, NSC-primed iPSC-macrophages did not achieve the same degree of ramification as compared to iPSC-microglia upon co-culture with NSCs (Fig. 3B versus Fig. 1A and D). Altogether, these results suggest that CX_3CR1^- ($eGFP^-$) iPSC-macrophages acquired new phenotypical properties as a result of the neural environment. Nonetheless, based on the degree of eGFP/CX_3CR1 expression, the morphological features, and the specific culture conditions – our results suggest that murine iPSC-microglia and NSC-primed iPSC-macrophages are intrinsically distinct cell populations.

3.4. *Murine iPSC-microglia, iPSC-macrophages and NSC-primed iPSC-macrophages differentially respond to classical pro-inflammatory stimulation*

As neuro-inflammatory lesions are initially characterised as a pro-inflammatory environment, we first investigated the activation properties of *in vitro* cultured murine iPSC-microglia, iPSC-macrophages and

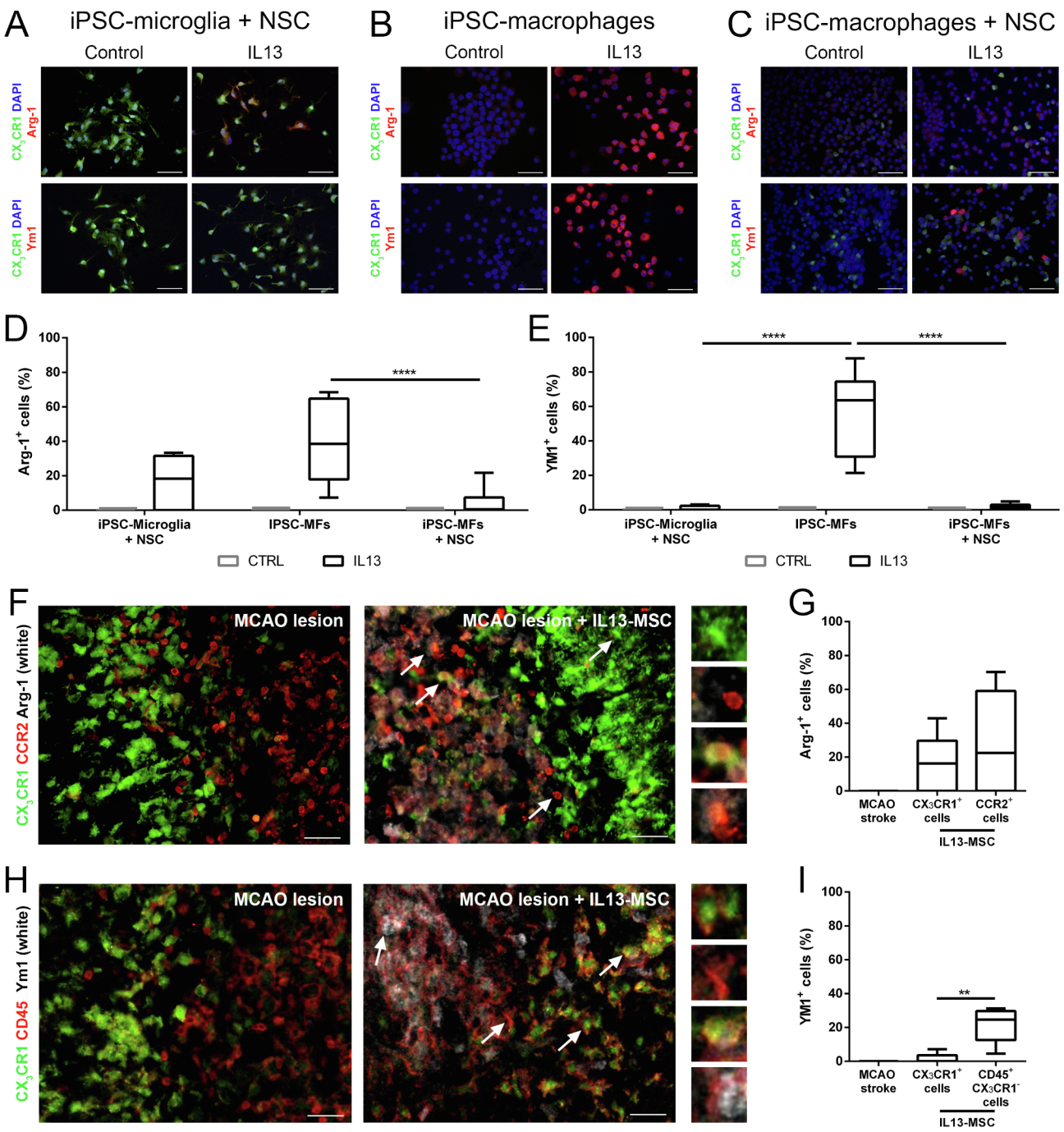

Fig. 5. Phenotypical properties of alternatively activated (IL13 stimulated) iPSC-microglia, iPSC-macrophages and NSC-primed iPSC-macrophages resemble the *in vivo* phenotypical profile of murine microglia and monocytes within IL-13 primed stroke lesions. Representative immunofluorescence images showing the expression of the markers Arginase-1 and Ym1 on A) iPSC-microglia in co-culture with NSCs, B) iPSC-macrophage monocultures and C) iPSC-macrophages in co-culture with NSCs under baseline culture conditions (control) and following stimulation with IL13. The secondary antibodies against Arginase-1 and Ym1 were coupled to Alexa Fluor 555 (red fluorescence), CX_3CR1 (eGFP) is directly visible as green fluorescence and nuclei are identified by DAPI staining (in blue). The scale bars indicate 50 µm. Quantitative analysis of the immunofluorescence images was performed for n = 3 per condition. Box plots showing the percentage of cells expressing D) Arginase-1 and E) Ym1 under control and IL13-stimulation conditions. Representative immunofluorescence images showing the expression of the markers F) Arginase-1 and H) Ym1 in a MCAO-induced brain lesion (left images) and in a MCAO-induced brain lesion following injection of IL13-expressing MSCs (right images) in $CX_3CR1^{eGFP/+}CCR2^{RFP/+}$ mice. White arrows indicate the illustrative close-up images (panel next to right image). The secondary antibody against Arginase-1 and Ym1 were coupled to Alexa Fluor350 (blue fluorescence) but shown here in white, the secondary antibody against RFP (associated with CCR2 expression) was coupled to Alexa Fluor 555 (red fluorescence), the antibody against CD45 (to identify infiltrating monocytes) was coupled to PE (red fluorescence) and CX_3CR1 (eGFP) expression is directly visible as green fluorescence. The scale bars indicate 100 µm. Quantitative analysis of the immunofluorescence images was performed on brain slices obtained from 5 mice. Box-plots showing the percentage of G) Arginase-1 and I) Ym1 expression within a MCAO-induced stroke lesion, and by CX_3CR1^+ cells and $CCR2^+/CD45^+CX_3CR1^-$ monocytes within a MCAO-induced stroke lesion following injection of IL13-expressing MSCs. Box plots indicate median and interquartile range, whiskers indicate the minimum and maximum values. **p < 0.01; ****p < 0.0001. Abbreviations: Arg-1, Arginase-1; CCR2, C–C chemokine receptor type 2; CX_3CR1, CX_3C chemokine receptor 1; CTRL, control; IL13, interleukin 13; iPSC, induced pluripotent stem cell; MCAO, middle cerebral arterial occlusion; MSC, mesenchymal stem cells; NSC, neural stem cell. (For interpretation of the references to colour in this figure legend, the reader is referred to the web version of this article.)

NSC-primed iPSC-macrophages by means of classical *in vitro* stimulation experiments. At baseline (control), all cell populations expressed similar low levels of the activation marker F4/80, which upon LPS + IFNγ stimulation was significantly increased for all cell populations (Fig. 4A-C upper row, Fig. 4D, respectively $p < 0.0001$, $p < 0.0001$ and $p = 0.00483$, p-values not indicated on graph). A remarkable observation was that the upregulation of F4/80 expression on iPSC-macrophages upon stimulation was significantly higher as compared to both iPSC-microglia (Fig. 4D, $p = 0.0003$) and NSC-primed iPSC-macrophages (Fig. 4D, $p < 0.0001$). In contrast, MHC-II expression was absent on all cell populations under control condition and was significantly upregulated by iPSC-macrophages and NSC-primed iPSC-macrophages following LPS + IFNγ treatment (Fig. 4A–C lower row, Fig. 4E, respectively $p < 0.0001$ and $p < 0.0001$), albeit the increase of MHCII expression only being of biological relevance for iPSC-macrophages. iPSC-microglia did not upregulate MHCII expression. In agreement with the F4/80 expression data, MHC-II expression by iPSC-macrophages was significantly higher as compared to stimulated iPSC-microglia (Fig. 4E, $p < 0.0001$) and NSC-primed iPSC-macrophages (Fig. 4E, $p < 0.0001$). These data demonstrate that the neural environment, apart from inducing morphological alterations and upregulation of CX_3CR1 expression, can also influence (part of) iPSC-macrophage functions. Furthermore, to complement the evaluation of the activation properties of iPSC-microglia, iPSC-macrophages and NSC-primed iPSC-macrophages, we also assessed cytokine secretion in both unstimulated and stimulated cultures. Significant levels of TNFα and IL6 secretion were produced in response to LPS + IFNγ for iPSC-microglia (Fig. 4F, G, respectively $p < 0.0001$ and $p < 0.0001$), iPSC-macrophages (Fig. 4F, G, respectively $p < 0.0001$ and $p < 0.0001$) and NSC-primed iPSC-macrophages (Fig. 4F, G, respectively $p < 0.0001$ and $p < 0.0001$). Interestingly, the immune-modulating cytokine IL10 was detected in the supernatant of LPS + IFNγ stimulated iPSC-microglia (Fig. 4H, $p < 0.0001$), iPSC-macrophages (Fig. 4H, $p = 0.0015$) and NSC-primed iPSC-macrophages (Fig. 4H, $p < 0.0001$), although the level of IL10 secretion can be considered biological relevant only for iPSC-microglia. None of the cytokines evaluated were produced by LPS + IFNγ stimulated NSCs (Fig. S2A–C).

3.5. Phenotypical properties of classically activated iPSC-microglia, iPSC-macrophages and NSC-primed iPSC-macrophages resemble the in vivo phenotypical profile of murine microglia and monocytes within stroke lesions

The above-described phenotypical differences between activated iPSC-microglia and iPSC-macrophages are fully in line with our preceding data concerning the behaviour of resident-microglia and infiltrating monocytes in course of a neuro-inflammatory event in $CX_3CR1^{eGFP/+}CCR2^{RFP/+}$ mice (Dooley et al., 2016; Hamzei Taj et al., 2018; Le Blon et al., 2016). In this section, we will further elaborate on the *in vivo* properties of microglia/monocytes within injured brain tissue after MCAO-stroke in $CX_3CR1^{eGFP/+}CCR2^{RFP/+}$ mice (Hamzei Taj et al., 2018). In contrast and complementing our previous study, we will specifically focus on the highly inflammatory MCAO lesion area, consisting of the core of the lesion and the immediate surrounding border where infiltrating monocytes are in close contact with resident microglia (previous analyses included a broader penumbra area). Furthermore, given the above-described data that iPSC-derived macrophages can acquire certain microglial characteristics (upregulation of CX_3CR1 expression), we will – within the MCAO stroke lesion in these $CX_3CR1^{eGFP/+}CCR2^{RFP/+}$ mice – consider CX_3CR1^{+} ($eGFP^{+}$) cells being either resident microglia or infiltrating monocytes that acquired microglial characteristics, while infiltrating monocytes that retained their original properties are characterised by the expression of CCR2 (RFP). Similar to the above-described *in vitro* experiments, we here evaluated the expression of F4/80 and MHCII. While expression of F4/80 or MHC-II was not observed on resting CX_3CR1^{+} microglia in the non-affected brain hemisphere (Fig. 4I and K left images; Fig. 4J and L), within the core of the lesion expression of F4/80 and MHCII was clearly present on both CX_3CR1^{+} microglia/monocytes and $CCR2^{+}$ monocytes (Fig. 4I and K right images; Fig. 4J and L). Strikingly similar to the above-described phenotypic analysis of activated murine iPSC-microglia, iPSC-macrophages and NSC-primed iPSC-macrophages (Fig. 4A–E), the number of F4/80 and MHCII expressing cells was significantly higher among the infiltrating $CCR2^{+}$ monocyte population as compared to the CX_3CR1^{+} microglia/monocytes population (Fig. 4J and L, respectively $p = 0.0292$ and $p < 0.0001$).

3.6. Murine iPSC-microglia, iPSC-macrophages and NSC-primed iPSC-macrophages differentially respond to IL13 stimulation

In contrast to LPS + IFNγ stimulation, which is considered to lead to nearly maximum pro-inflammatory (classical) activation, the immune modulating cytokine IL13 is considered to promote nearly maximum alternative activation. The latter, at least for macrophages, is characterised by the upregulation of Arginase-1 and Ym1 proteins. In this part of our study, we investigated the response of murine iPSC-microglia, iPSC-macrophages and NSC-primed iPSC-macrophages to IL13 stimulation. For Arginase-1 no expression was detected in iPSC-microglia, iPSC-macrophages and NSC-primed iPSC-macrophages under control conditions. As expected both iPSC-microglia and iPSC-macrophages were able to respond to IL13 signalling and express Arginase-1, without significant difference between both populations (Fig. 5A–C, upper row; and Fig. 5D). Interestingly, the presence of a neural environment significantly reduced the number of Arginase-1 expressing cells in NSC-primed iPSC-macrophage cultures as compared to iPSC-macrophage monocultures (Fig. 5D, $p < 0.0001$). For Ym1, while no expression was detected in iPSC-microglia, iPSC-macrophages and NSC-primed iPSC-macrophages under control conditions, iPSC-macrophages, but not iPSC-microglia, were able to induce Ym1 expression in response to IL13 signalling (Fig. 5C, lower row; and Fig. 5E, $p < 0.0001$). Again of high interest, the presence of a neural environment nearly abolished the number of Ym1 expressing cells in NSC-primed iPSC-macrophage cultures as compared to iPSC-macrophage cultures (Fig. 5E, $p < 0.0001$). In summary, while iPSC-macrophages upregulated both Arginase-1 and Ym1 upon IL13 stimulation, iPSC-microglia only upregulated Arginase-1 expression. Furthermore, the presence of a neural environment inhibits expression of both Arginase-1 and Ym1 by iPSC-macrophages during IL13 stimulation.

3.7. Phenotypical properties of alternatively activated (IL13 stimulated) iPSC-microglia, iPSC-macrophages and NSC-primed iPSC-macrophages resemble the in vivo phenotypical profile of murine microglia and monocytes within IL-13 primed stroke lesions

In previous studies using $CX_3CR1^{eGFP/+}CCR2^{RFP/+}$ mice, we have shown that therapeutic delivery of IL13, by means of lentiviral vector injection or implantation of genetically modified MSC, can efficiently induce Arginase-1 expression in microglia and infiltrating monocytes in experimental models of cuprizone-induced demyelination (Le Blon et al., 2016), spinal cord injury (Dooley et al., 2016) and stroke (Hamzei Taj et al., 2018), albeit – in general – with a higher efficiency in the CNS infiltrating monocyte population as compared to the microglia population. In this new study we also evaluated Ym1 as an additional marker for alternative activation, and thus performed additional analyses to investigate whether expression of Arginase-1 by IL13-primed microglia and infiltrating monocytes within the core of an MCAO lesion coincides with Ym1 expression. Similar to the analyses described above, we here specifically focused on the highly inflammatory MCAO lesion area, consisting of the core of the lesion and the immediate surrounding border; in case of therapeutic IL13 delivery, the area directly adjacent to the injection site was evaluated (thereby assuring effective delivery of the IL13 protein). As expected, in control $CX3CR1^{eGFP/+}CCR2^{RFP/+}$ mice with MCAO stroke, both Arginase-1 and

Ym1 expression was absent within the pro-inflammatory lesion environment (Fig. 5F and H, left images; Fig. 5G and I). Following therapeutic delivery of IL13, Arginase-1 expressing CX_3CR1^+ microglia/monocytes and $CCR2^+$ monocytes were clearly present, without significant difference between both populations (Fig. 5F, right image; Fig. 5G). In contrast, and strikingly similar to the above-described phenotypic analysis of IL13 stimulated iPSC-microglia, iPSC-macrophages and NSC-primed iPSC-macrophages (Fig. 5A-E), Ym1 expression was significantly higher on $CD45^+CX_3CR1^-$ ($CCR2^+$) monocytes as compared to $CD45^+CX_3CR1^+$ microglia/monocytes (Fig. 5H, right image; Fig. 5I, $p = 0.00127$). In summary, these findings demonstrate that within an IL13-primed MCAO stroke lesion the induction of the full alternative activation program, as characterized by both Arginase-1 and Ym1 expression, was more evident on infiltrating monocytes, while resident microglia or infiltrating monocytes that acquired microglial characteristics (CX_3CR1 expression) were only able to induce Arginase-1 expression, but not Ym1 expression. Clearly, the influence of the neural environment *in vivo* should not be underestimated, as shown above during IL13 stimulation experiments of iPSC-microglia, iPSC-macrophages and NSC-primed iPSC-macrophages.

4. Discussion

Reliable *in vitro* models to study and modulate neuroinflammation are essential instruments for pre-clinical design and validation of novel therapeutic approaches for CNS disorders where inflammation plays a major role in the pathogenic process. Until the past decade, *in vitro* studies of microglial biology have been strongly hindered by the difficulty in acquiring primary microglia cells, as well as the unreliability of the available microglia cell lines (Butovsky et al., 2014; Stansley et al., 2012; Timmerman et al., 2018). More recently, a growing interest in studying microglia's role in multiple brain disorders has brought this cell population in the spotlight of stem cell research. As a consequence, several groups developed efficient methods to differentiate murine and human microglia(-like) cells from iPSC, thereby generating a new and unlimited source of microglia cells for *in vitro* research (Abud et al., 2017; Brownjohn et al., 2018; Claes et al., 2019; Douvaras et al., 2017; Garcia-Reitboeck et al., 2018; Haenseler et al., 2017; McQuade et al., 2018; Muffat et al., 2016; Pandya et al., 2017; Takata et al., 2017). In the current work we applied an iPSC-microglia differentiation protocol based on procedures reported in recent literature (Brownjohn et al., 2018; Douvaras et al., 2017; Pandya et al., 2017). To this end, ramified CX_3CR1^+ ($eGFP^+$) murine iPSC-microglia were cultured and analysed in co-culture with astrocyte-committed embryonic brain-derived NSCs, which provided the environmental cues necessary to sustain microglia identity *in vitro* (Bohlen et al., 2017; Butovsky et al., 2014).

Beside microglia, also brain infiltrating monocytes play a major role both in the pathogenesis and in the resolution of neuroinflammatory responses (Ajami et al., 2011; Hamzei Taj et al., 2018; Morganti et al., 2015; Ritzel et al., 2015; Varvel et al., 2016; Yamasaki et al., 2014). At sites of inflammation, monocytes rapidly exit the circulatory system and reach the inflamed CNS driven by signalling via the chemokine receptor CCR2 (Ginhoux and Jung, 2014). Consequently, their half-life in the circulatory compartment is restricted to only 20 h, while the lifespan of tissue-resident macrophages is significantly larger (Ginhoux and Jung, 2014). At current, there are no *in vitro* protocols available for the specific generation of murine $CCR2^+$ monocytes from iPSC. Therefore, in the current work we applied an iPSC-macrophage differentiation protocol based on procedures well-reported in literature (Zhuang et al., 2012) and obtained CX_3CR1^- $CCR2^-$ round-shaped murine macrophages that were considered as *in vitro* equivalent of blood-derived monocytes. Obviously future research directions may need to focus on identifying bone marrow and/or blood-derived factors that allow establishment and/or maintenance of CX_3CR1^- $CCR2^+$ monocyte identity *in vitro*. At current, our attempts to achieve the latter were unsuccessful.

Recent transcriptomic studies highlighted that both developmental and environmental factors cooperate in establishing specific identity of different populations of tissue-resident macrophages (Bennett et al., 2018; Gosselin et al., 2014; Lund et al., 2018). Although microglia are most distinct from other tissue-resident macrophages in terms of genetic landscape, macrophage populations that are exposed to similar environmental cues as microglia may converge to similar expression patterns and acquire similar morphological and phenotypical features (Abutbul et al., 2012; Bennett et al., 2018; Etemad et al., 2012; Hinze and Stolzing, 2011; Lund et al., 2018; Noto et al., 2014). Stimulated by these observations, we investigated to what extent a neural environment was able to influence the behaviour of our cultured murine iPSC-macrophages. A first finding described in this study was the ability of iPSC-macrophages to partially modify their morphological and phenotypical properties following culture on OBSCs or NSCs. Nevertheless, NSC-primed iPSC-macrophages were not equivalent to iPSC-microglia both in morphology and in the level of CX_3CR1 expression, thereby indicating that the iPSC-microglia and iPSC-macrophages used to perform our studies are clearly distinct cell populations. It should however be stressed that we studied murine iPSC-microglia behaviour exclusively within a neural environment. While culturing microglia in absence of other brain cells is certainly technically convenient, it may produce deviating results from the actual *in vivo* situation. Indeed, it is increasingly recognised that cross-talk with CNS cells is required to maintain microglia transcriptional signature *in vitro* (Bennett et al., 2018; Bohlen et al., 2017; Butovsky et al., 2014; Neiva et al., 2014). In this context, the functional data presented in this manuscript also suggest that a culture system mimicking the brain milieu, in this study using astrocyte-committed embryonic-brain derived NSC, is essential to reproduce *in vitro* physiologically relevant murine microglia behaviour.

As described in the introductory section, studying neuro-inflammatory responses should consider both microglia and monocytes/macrophages. To our best knowledge, our study is the first comparative study of murine iPSC-microglia with iPSC-macrophages and to a further extent with their *in vivo* counterpart. Given our specific interest, we here focused on classical and alternative activation of iPSC-microglia and iPSC-macrophages. To investigate the response of iPSC-microglia and iPSC-macrophages to pro-inflammatory polarisation, we performed *in vitro* stimulation with LPS + IFNγ. Here we observed that iPSC-macrophages, iPSC-microglia and NSC-primed iPSC macrophages were equally susceptible to this trigger as confirmed by the secretion of pro-inflammatory cytokines, although iPSC-microglia may be less prone to the known IFNγ mediated inhibition of IL10 secretion by macrophages (Flores et al., 2007; Hu et al., 2006; Lively and Schlichter, 2018). In contrast, the expression of the activation markers F4/80 and MHCII was significantly higher on iPSC-macrophages as compared to iPSC-microglia and NSC-primed iPSC macrophages. Especially for MHCII expression, this may have several implications. At one end, it may signify a brain tissue-specific negative feedback in order to avoid antigen presentation to $CD4^+$ T-cells and subsequently avoiding auto-immunity to brain-specific antigens. On the other hand, inhibition of MHCII expression on antigen-presenting cells may limit adaptive immunity to CNS-derived tumours (Jurewicz and Stern, 2019; Rock et al., 2016). To investigate whether murine iPSC-microglia and iPSC-macrophages could be directed into a stage of alternative activation, we performed *in vitro* stimulation with IL13. While iPSC-macrophages as expected upregulated both Arginase-1 and Ym1 upon IL13 stimulation, iPSC-microglia only upregulated Arginase-1 expression. Of high biological relevance is our observation that the neural environment is able to inhibit expression of both Arginase-1 and Ym1 by iPSC-macrophages during IL13 stimulation. While lack of Arginase-1 expression can clearly be linked to the inability of macrophages to counteract signals promoting nitric oxide (NO) production (Rath et al., 2014; Roszer, 2015), lack of Ym1 expression may limit their wound healing and tissue remodelling properties (Hung et al., 2002; Mosser and Edwards, 2008).

Following these data, it is highly suggestive that the neural

environment restricts not only the classical activation potential of murine iPSC-microglia and iPSC-macrophages cultured within a neural environment, but also their alternative activation which is considered to counteract the inflammatory environment and promote tissue regeneration. Several signalling pathways able to maintain microglia in a quiescent state *in vivo* are described in literature, for example by means of multiple interactions with neurons (CX_3CR1-CX_3CL1 and CD200R-CD200) and astrocytes (TGF-βR-TGF-β) (Abutbul et al., 2012; Cardona et al., 2006; De Vocht et al., 2013; Manich et al., 2019; Neiva et al., 2014). Since our iPSC-microglia culture system involves co-culture with astrocyte-committed NSC, in a preliminary experiment we attempted to inhibit TGF-β signalling during classical and alternative immune polarisation, however no alterations were observed. Further investigation into this topic is of high relevance in the context of immuno-modulating therapeutic strategies as it should indicate whether or not microglia can be triggered in the same alternative and/or regeneration-inducing phenotype as already established for iPSC-derived macrophages. If only infiltrating monocytes are truly able to acquire a sustained anti-inflammatory phenotype, as suggested by our *in vivo* and *in vitro* findings, the use of immune-modulating agents will be effective only for CNS disorders characterized by a major influx of blood-derived cells to the brain. Alternatively, the administration of M2-inducing compounds should be associated with an additional intervention designed to unlock the alternative activation potential of microglia.

Finally, we would like to stress our *in vivo* validation approach whereby we demonstrate that the distinct phenotypical properties of *in vitro* stimulated murine iPSC-microglia and iPSC-macrophages closely resemble the activation profile observed *in vivo* for endogenous microglia and infiltrating monocytes following MCAO stroke and IL13-based therapeutic intervention thereon. This is an important result which validates the presented murine iPSC model as suitable instrument for future preclinical studies. As such, we propose the use of murine iPSC-microglia (corresponding to brain-resident microglia), iPSC-macrophages (corresponding to CNS infiltrating monocytes) and NSC-primed iPSC-macrophages (corresponding to CNS infiltrating monocytes that acquired a microglia-like phenotype) to identify and study novel cellular targets to modulate neuro-inflammatory responses. *In vitro* cellular models are especially convenient for screening large libraries of compounds as well as for fine-tuning studies, such as the identification of specific mechanism of action and signalling pathways. Notwithstanding, it is important to underline that the cellular response to an inflammatory trigger is regulated by a combination of local signalling and systemic factors. As *in vitro* systems do not allow to evaluate complex systemic responses, it will remain crucial to also investigate the efficacy of potential novel therapeutic agents *in vivo* using appropriate animal models of disease.

5. Conclusions

In this work we have established and validated three murine cell culture models, iPSC-microglia, iPSC-macrophages and NSC-primed iPSC-macrophages that are able to recapitulate the pro-inflammatory and anti-inflammatory phenotypic properties of brain-resident microglia and infiltrating monocytes during an inflammatory insult (MCAO stroke), as well as following IL13-based therapeutic intervention thereon. The striking resemblance of the functional properties of immune cells studied *in vitro* and *in vivo* highlights the future possibilities and applications of iPSC-derived neuro-immune cell culture models in both fundamental and applied neuroinflammation research.

Acknowledgments and funding sources

This work was supported by research grant G091518N (granted to PP) of the Fund for Scientific Research-Flanders (FWO-Vlaanderen, Belgium), by a Methusalem research grant from the Flemish government (granted to HG and ZB), by funding received from the Belgian Charcot Foundation (granted to PP and DLB) and by the ASCID (Antwerp Study Centre for Infectious Diseases). AQ and EL are holders of a PhD studentship from the FWO-Vlaanderen. EVB is holder of a PhD studentship from the University of Antwerp. DLB is holder of a post-doctoral fellowship from the FWO-Vlaanderen. FM is supported by the Peris 2016 from the Health Department of Generalitat de Catalunya. Research in the Pasque lab is supported by the Research Foundation – Flanders (FWO) (Odysseus Return Grant G0F7716N, to V.P.), the KU Leuven Research Fund (BOFZAP starting grant StG/15/021BF to V.P. C1 grant C14/16/077 to V.P. and Project financing).

Appendix A. Supplementary data

Supplementary data to this article can be found online at https://doi.org/10.1016/j.bbi.2019.09.009.

References

Abud, E.M., Ramirez, R.N., Martinez, E.S., Healy, L.M., Nguyen, C.H.H., Newman, S.A., Yeromin, A.V., Scarfone, V.M., Marsh, S.E., Fimbres, C., Caraway, C.A., Fote, G.M., Madany, A.M., Agrawal, A., Kayed, R., Gylys, K.H., Cahalan, M.D., Cummings, B.J., Antel, J.P., Mortazavi, A., Carson, M.J., Poon, W.W., Blurton-Jones, M., 2017. iPSC-derived human microglia-like cells to study neurological diseases. Neuron 94 1170–1183 e279.

Abutbul, S., Shapiro, J., Szaingurten-Solodkin, I., Levy, N., Carmy, Y., Baron, R., Jung, S., Monsonego, A., 2012. TGF-beta signaling through SMAD2/3 induces the quiescent microglial phenotype within the CNS environment. Glia 60, 1160–1171.

Ajami, B., Bennett, J.L., Krieger, C., McNagny, K.M., Rossi, F.M., 2011. Infiltrating monocytes trigger EAE progression, but do not contribute to the resident microglia pool. Nat. Neurosci. 14, 1142–1149.

Benjamini, Y., Hochberg, Y., 1995. Controlling the false discovery rate – a practical and powerful approach to multiple testing. J R Stat Soc B 57, 289–300.

Bennett, M.L., Bennett, F.C., Liddelow, S.A., Ajami, B., Zamanian, J.L., Fernhoff, N.B., Mulinyawe, S.B., Bohlen, C.J., Adil, A., Tucker, A., Weissman, I.L., Chang, E.F., Li, G., Grant, G.A., Hayden Gephart, M.G., Barres, B.A., 2016. New tools for studying microglia in the mouse and human CNS. Proc. Natl. Acad. Sci. USA 113, E1738–E1746.

Bennett, F.C., Bennett, M.L., Yaqoob, F., Mulinyawe, S.B., Grant, G.A., Hayden Gephart, M., Plowey, E.D., Barres, B.A., 2018. A combination of ontogeny and CNS environment establishes microglial identity. Neuron 98 1170–1183 e1178.

Beutner, C., Roy, K., Linnartz, B., Napoli, I., Neumann, H., 2010. Generation of microglial cells from mouse embryonic stem cells. Nat. Protoc. 5, 1481–1494.

Bohlen, C.J., Bennett, F.C., Tucker, A.F., Collins, H.Y., Mulinyawe, S.B., Barres, B.A., 2017. Diverse requirements for microglial survival, specification, and function revealed by defined-medium cultures. Neuron 94 (759–773), e758.

Brownjohn, P.W., Smith, J., Solanki, R., Lohmann, E., Houlden, H., Hardy, J., Dietmann, S., Livesey, F.J., 2018. Functional studies of missense TREM2 mutations in human stem cell-derived microglia. Stem Cell Rep. 10, 1294–1307.

Butovsky, O., Jedrychowski, M.P., Moore, C.S., Cialic, R., Lanser, A.J., Gabriely, G., Koeglsperger, T., Dake, B., Wu, P.M., Doykan, C.E., Fanek, Z., Liu, L., Chen, Z., Rothstein, J.D., Ransohoff, R.M., Gygi, S.P., Antel, J.P., Weiner, H.L., 2014. Identification of a unique TGF-beta-dependent molecular and functional signature in microglia. Nat. Neurosci. 17, 131–143.

Cardona, A.E., Pioro, E.P., Sasse, M.E., Kostenko, V., Cardona, S.M., Dijkstra, I.M., Huang, D., Kidd, G., Dombrowski, S., Dutta, R., Lee, J.C., Cook, D.N., Jung, S., Lira, S.A., Littman, D.R., Ransohoff, R.M., 2006. Control of microglial neurotoxicity by the fractalkine receptor. Nat. Neurosci. 9, 917–924.

Cherry, J.D., Olschowka, J.A., O'Banion, M.K., 2014. Neuroinflammation and M2 microglia: the good, the bad, and the inflamed. J. Neuroinflammation 11, 98.

Claes, C., Van Den Daele, J., Boon, R., Schouteden, S., Colombo, A., Monasor, L.S., Fiers, M., Ordovas, L., Nami, F., Bohrmann, B., Tahirovic, S., De Strooper, B., Verfaillie, C.M., 2019. Human stem cell-derived monocytes and microglia-like cells reveal impaired amyloid plaque clearance upon heterozygous or homozygous loss of TREM2. Alzheimers Dement. 15, 453–464.

Costa, R., Bergwerf, I., Santermans, E., De Vocht, N., Praet, J., Daans, J., Le Blon, D., Hoornaert, C., Reekmans, K., Hens, N., Goossens, H., Berneman, Z., Parolini, O., Alviano, F., Ponsaerts, P., 2015. Distinct in vitro properties of embryonic and extraembryonic fibroblast-like cells are reflected in their in vivo behavior following grafting in the adult mouse brain. Cell Transplant. 24, 223–233.

De Vocht, N., Praet, J., Reekmans, K., Le Blon, D., Hoornaert, C., Daans, J., Berneman, Z., Van der Linden, A., Ponsaerts, P., 2013. Tackling the physiological barriers for successful mesenchymal stem cell transplantation into the central nervous system. Stem Cell Res. Ther. 4, 101.

DiSabato, D.J., Quan, N., Godbout, J.P., 2016. Neuroinflammation: the devil is in the details. J. Neurochem. 139 (Suppl 2), 136–153.

Dooley, D., Lemmens, E., Vangansewinkel, T., Le Blon, D., Hoornaert, C., Ponsaerts, P., Hendrix, S., 2016. Cell-based delivery of interleukin-13 directs alternative activation of macrophages resulting in improved functional outcome after spinal cord injury. Stem Cell Rep. 7, 1099–1115.

Douvaras, P., Sun, B., Wang, M., Kruglikov, I., Lallos, G., Zimmer, M., Terrenoire, C., Zhang, B., Gandy, S., Schadt, E., Freytes, D.O., Noggle, S., Fossati, V., 2017. Directed

differentiation of human pluripotent stem cells to microglia. Stem Cell Rep. 8, 1516–1524.
Etemad, S., Zamin, R.M., Ruitenberg, M.J., Filgueira, L., 2012. A novel in vitro human microglia model: characterization of human monocyte-derived microglia. J. Neurosci. Methods 209, 79–89.
Flores, R.R., Diggs, K.A., Tait, L.M., Morel, P.A., 2007. IFN-gamma negatively regulates CpG-induced IL-10 in bone marrow-derived dendritic cells. J. Immunol. 178, 211–218.
Garcia-Reitboeck, P., Phillips, A., Piers, T.M., Villegas-Llerena, C., Butler, M., Mallach, A., Rodrigues, C., Arber, C.E., Heslegrave, A., Zetterberg, H., Neumann, H., Neame, S., Houlden, H., Hardy, J., Pocock, J.M., 2018. Human induced pluripotent stem cell-derived microglia-like cells harboring TREM2 missense mutations show specific deficits in phagocytosis. Cell Rep 24, 2300–2311.
Ginhoux, F., Greter, M., Leboeuf, M., Nandi, S., See, P., Gokhan, S., Mehler, M.F., Conway, S.J., Ng, L.G., Stanley, E.R., Samokhvalov, I.M., Merad, M., 2010. Fate mapping analysis reveals that adult microglia derive from primitive macrophages. Science 330, 841–845.
Ginhoux, F., Jung, S., 2014. Monocytes and macrophages: developmental pathways and tissue homeostasis. Nat. Rev. Immunol. 14, 392–404.
Gosselin, D., Link, V.M., Romanoski, C.E., Fonseca, G.J., Eichenfield, D.Z., Spann, N.J., Stender, J.D., Chun, H.B., Garner, H., Geissmann, F., Glass, C.K., 2014. Environment drives selection and function of enhancers controlling tissue-specific macrophage identities. Cell 159, 1327–1340.
Guglielmetti, C., Le Blon, D., Santermans, E., Salas-Perdomo, A., Daans, J., De Vocht, N., Shah, D., Hoornaert, C., Praet, J., Peerlings, J., Kara, F., Bigot, C., Mai, Z., Goossens, H., Hens, N., Hendrix, S., Verhoye, M., Planas, A.M., Berneman, Z., van der Linden, A., Ponsaerts, P., 2016. Interleukin-13 immune gene therapy prevents CNS inflammation and demyelination via alternative activation of microglia and macrophages. Glia 64, 2181–2200.
Gupta, N., Shyamasundar, S., Patnala, R., Karthikeyan, A., Arumugam, T.V., Ling, E.A., Dheen, S.T., 2018. Recent progress in therapeutic strategies for microglia-mediated neuroinflammation in neuropathologies. Expert Opin. Ther. Targets 22, 765–781.
Haenseler, W., Sansom, S.N., Buchrieser, J., Newey, S.E., Moore, C.S., Nicholls, F.J., Chintawar, S., Schnell, C., Antel, J.P., Allen, N.D., Cader, M.Z., Wade-Martins, R., James, W.S., Cowley, S.A., 2017. A highly efficient human pluripotent stem cell microglia model displays a neuronal-co-culture-specific expression profile and inflammatory response. Stem Cell Rep. 8, 1727–1742.
Hamzei Taj, S., Le Blon, D., Hoornaert, C., Daans, J., Quarta, A., Praet, J., Van der Linden, A., Ponsaerts, P., Hoehn, M., 2018. Targeted intracerebral delivery of the anti-inflammatory cytokine IL13 promotes alternative activation of both microglia and macrophages after stroke. J. Neuroinflammation 15, 174.
Hinze, A., Stolzing, A., 2011. Differentiation of mouse bone marrow derived stem cells toward microglia-like cells. BMC Cell Biol 12, 35.
Hoeffel, G., Chen, J., Lavin, Y., Low, D., Almeida, F.F., See, P., Beaudin, A.E., Lum, J., Low, I., Forsberg, E.C., Poidinger, M., Zolezzi, F., Larbi, A., Ng, L.G., Chan, J.K., Greter, M., Becher, B., Samokhvalov, I.M., Merad, M., Ginhoux, F., 2015. C-Myb(+) erythro-myeloid progenitor-derived fetal monocytes give rise to adult tissue-resident macrophages. Immunity 42, 665–678.
Hoornaert, C.J., Luyckx, E., Reekmans, K., Dhainaut, M., Guglielmetti, C., Le Blon, D., Dooley, D., Fransen, E., Daans, J., Verbeeck, L., Quarta, A., De Vocht, N., Lemmens, E., Goossens, H., Van der Linden, A., Roobrouck, V.D., Verfaillie, C., Hendrix, S., Moser, M., Berneman, Z.N., Ponsaerts, P., 2016. In vivo interleukin-13-primed macrophages contribute to reduced alloantigen-specific T cell activation and prolong immunological survival of allogeneic mesenchymal stem cell implants. Stem Cells 34, 1971–1984.
Hu, X., Paik, P.K., Chen, J., Yarilina, A., Kockeritz, L., Lu, T.T., Woodgett, J.R., Ivashkiv, L.B., 2006. IFN-gamma suppresses IL-10 production and synergizes with TLR2 by regulating GSK3 and CREB/AP-1 proteins. Immunity 24, 563–574.
Hu, X., Leak, R.K., Shi, Y., Suenaga, J., Gao, Y., Zheng, P., Chen, J., 2015. Microglial and macrophage polarization-new prospects for brain repair. Nat. Rev. Neurol. 11, 56–64.
Hung, S.I., Chang, A.C., Kato, I., Chang, N.C., 2002. Transient expression of Ym1, a heparin-binding lectin, during developmental hematopoiesis and inflammation. J. Leukoc. Biol. 72, 72–82.
Italiani, P., Boraschi, D., 2014. From monocytes to M1/M2 macrophages: phenotypical vs functional differentiation. Front. Immunol. 5, 514.
Jurewicz, M.M., Stern, L.J., 2019. Class II MHC antigen processing in immune tolerance and inflammation. Immunogenetics 71, 171–187.
Kanazawa, M., Ninomiya, I., Hatakeyama, M., Takahashi, T., Shimohata, T., 2017. Microglia and monocytes/macrophages polarization reveal novel therapeutic mechanism against stroke. Int. J. Mol. Sci. 18.
Kierdorf, K., Erny, D., Goldmann, T., Sander, V., Schulz, C., Perdiguero, E.G., Wieghofer, P., Heinrich, A., Riemke, P., Holscher, C., Muller, D.N., Luckow, B., Brocker, T., Debowski, K., Fritz, G., Opdenakker, G., Diefenbach, A., Biber, K., Heikenwalder, M., Geissmann, F., Rosenbauer, F., Prinz, M., 2013. Microglia emerge from erythromyeloid precursors via Pu.1- and Irf8-dependent pathways. Nat. Neurosci. 16, 273–280.
Koeniger, T., Kuerten, S., 2017. Splitting the “Unsplittable”: dissecting resident and infiltrating macrophages in experimental autoimmune encephalomyelitis. Int. J. Mol. Sci. 18.
Kong, X., Gao, J., 2017. Macrophage polarization: a key event in the secondary phase of acute spinal cord injury. J. Cell Mol. Med. 21, 941–954.
Kronenberg, G., Uhlemann, R., Richter, N., Klempin, F., Wegner, S., Staerck, L., Wolf, S., Uckert, W., Kettenmann, H., Endres, M., Gertz, K., 2018. Distinguishing features of microglia- and monocyte-derived macrophages after stroke. Acta Neuropathol. 135, 551–568.
Kumar, A., Alvarez-Croda, D.M., Stoica, B.A., Faden, A.I., Loane, D.J., 2016. Microglial/macrophage polarization dynamics following traumatic brain injury. J. Neurotrauma 33, 1732–1750.
Le Blon, D., Guglielmetti, C., Hoornaert, C., Quarta, A., Daans, J., Dooley, D., Lemmens, E., Praet, J., De Vocht, N., Reekmans, K., Santermans, E., Hens, N., Goossens, H., Verhoye, M., Van der Linden, A., Berneman, Z., Hendrix, S., Ponsaerts, P., 2016. Intracerebral transplantation of interleukin 13-producing mesenchymal stem cells limits microgliosis, oligodendrocyte loss and demyelination in the cuprizone mouse model. J. Neuroinflammation 13, 288.
Lively, S., Schlichter, L.C., 2018. Microglia responses to pro-inflammatory stimuli (LPS, IFNgamma+TNFalpha) and reprogramming by resolving cytokines (IL-4, IL-10). Front. Cell. Neurosci. 12, 215.
Lund, H., Pieber, M., Parsa, R., Han, J., Grommisch, D., Ewing, E., Kular, L., Needhamsen, M., Espinosa, A., Nilsson, E., Overby, A.K., Butovsky, O., Jagodic, M., Zhang, X.M., Harris, R.A., 2018. Competitive repopulation of an empty microglial niche yields functionally distinct subsets of microglia-like cells. Nat. Commun. 9, 4845.
Luyckx, E., Van Leuven, W., Andre, D., Quarta, A., Reekmans, K., Fransen, E., Moens, L., Hankeln, T., Ponsaerts, P., Dewilde, S., 2018. Loss of neuroglobin expression alters Cdkn1a/Cdk6-expression resulting in increased proliferation of neural stem cells. Stem Cells Dev. 27, 378–390.
Manich, G., Recasens, M., Valente, T., Almolda, B., Gonzalez, B., Castellano, B., 2019. Role of the CD200-CD200R axis during homeostasis and neuroinflammation. Neuroscience 405, 118–136.
Masuch, A., van der Pijl, R., Funer, L., Wolf, Y., Eggen, B., Boddeke, E., Biber, K., 2016. Microglia replenished OHSC: A culture system to study in vivo like adult microglia. Glia 64, 1285–1297.
McQuade, A., Coburn, M., Tu, C.H., Hasselmann, J., Davtyan, H., Blurton-Jones, M., 2018. Development and validation of a simplified method to generate human microglia from pluripotent stem cells. Mol. Neurodegener. 13, 67.
Milich, L.M., Ryan, C.B., Lee, J.K., 2019. The origin, fate, and contribution of macrophages to spinal cord injury pathology. Acta Neuropathol. 137, 785–797.
Morganti, J.M., Jopson, T.D., Liu, S., Riparip, L.K., Guandique, C.K., Gupta, N., Ferguson, A.R., Rosi, S., 2015. CCR2 antagonism alters brain macrophage polarization and ameliorates cognitive dysfunction induced by traumatic brain injury. J. Neurosci. 35, 748–760.
Mosser, D.M., Edwards, J.P., 2008. Exploring the full spectrum of macrophage activation. Nat. Rev. Immunol. 8, 958–969.
Muffat, J., Li, Y., Yuan, B., Mitalipova, M., Omer, A., Corcoran, S., Bakiasi, G., Tsai, L.H., Aubourg, P., Ransohoff, R.M., Jaenisch, R., 2016. Efficient derivation of microglia-like cells from human pluripotent stem cells. Nat. Med. 22, 1358–1367.
Murray, P.J., 2017. Macrophage polarization. Annu. Rev. Physiol. 79, 541–566.
Neiva, I., Malva, J.O., Valero, J., 2014. Can we talk about microglia without neurons? A discussion of microglial cell autonomous properties in culture. Front. Cell. Neurosci. 8, 202.
Noto, D., Sakuma, H., Takahashi, K., Saika, R., Saga, R., Yamada, M., Yamamura, T., Miyake, S., 2014. Development of a culture system to induce microglia-like cells from haematopoietic cells. Neuropathol. Appl. Neurobiol. 40, 697–713.
Orihuela, R., McPherson, C.A., Harry, G.J., 2016. Microglial M1/M2 polarization and metabolic states. Br. J. Pharmacol. 173, 649–665.
Pandya, H., Shen, M.J., Ichikawa, D.M., Sedlock, A.B., Choi, Y., Johnson, K.R., Kim, G., Brown, M.A., Elkahloun, A.G., Maric, D., Sweeney, C.L., Gossa, S., Malech, H.L., McGavern, D.B., Park, J.K., 2017. Differentiation of human and murine induced pluripotent stem cells to microglia-like cells. Nat. Neurosci. 20, 753–759.
Pasque, V., Tchieu, J., Karnik, R., Uyeda, M., Sadhu Dimashkie, A., Case, D., Papp, B., Bonora, G., Patel, S., Ho, R., Schmidt, R., McKee, R., Sado, T., Tada, T., Meissner, A., Plath, K., 2014. X chromosome reactivation dynamics reveal stages of reprogramming to pluripotency. Cell 159, 1681–1697.
Pedragosa, J., Salas-Perdomo, A., Gallizioli, M., Cugota, R., Miro-Mur, F., Brianso, F., Justicia, C., Perez-Asensio, F., Marquez-Kisinousky, L., Urra, X., Gieryng, A., Kaminska, B., Chamorro, A., Planas, A.M., 2018. CNS-border associated macrophages respond to acute ischemic stroke attracting granulocytes and promoting vascular leakage. Acta Neuropathol. Commun. 6, 76.
Praet, J., Santermans, E., Reekmans, K., de Vocht, N., Le Blon, D., Hoornaert, C., Daans, J., Goossens, H., Berneman, Z., Hens, N., Van der Linden, A., Ponsaerts, P., 2014. Histological characterization and quantification of cellular events following neural and fibroblast(-like) stem cell grafting in healthy and demyelinated CNS tissue. Methods Mol. Biol. 1213, 265–283.
Prinz, M., Priller, J., 2014. Microglia and brain macrophages in the molecular age: from origin to neuropsychiatric disease. Nat. Rev. Neurosci. 15, 300–312.
Rajkovic, O., Potjewyd, G., Pinteaux, E., 2018. Regenerative medicine therapies for targeting neuroinflammation after stroke. Front. Neurol. 9, 734.
Ransohoff, R.M., Perry, V.H., 2009. Microglial physiology: unique stimuli, specialized responses. Annu. Rev. Immunol. 27, 119–145.
Rath, M., Muller, I., Kropf, P., Closs, E.I., Munder, M., 2014. Metabolism via arginase or nitric oxide synthase: two competing arginine pathways in macrophages. Front. Immunol. 5, 532.
Reekmans, K., De Vocht, N., Praet, J., Le Blon, D., Hoornaert, C., Daans, J., Van der Linden, A., Berneman, Z., Ponsaerts, P., 2013. Quantitative evaluation of stem cell grafting in the central nervous system of mice by in vivo bioluminescence imaging and postmortem multicolor histological analysis. Methods Mol. Biol. 1052, 125–141.
Reekmans, K.P., Praet, J., De Vocht, N., Tambuyzer, B.R., Bergwerf, I., Daans, J., Baekelandt, V., Vanhoutte, G., Goossens, H., Jorens, P.G., Ysebaert, D.K., Chatterjee, S., Pauwels, P., Van Marck, E., Berneman, Z.N., Van der Linden, A., Ponsaerts, P., 2011. Clinical potential of intravenous neural stem cell delivery for treatment of neuroinflammatory disease in mice? Cell Transplant. 20, 851–869.
Ritzel, R.M., Patel, A.R., Grenier, J.M., Crapser, J., Verma, R., Jellison, E.R., McCullough, L.D., 2015. Functional differences between microglia and monocytes after ischemic

stroke. J. Neuroinflammation 12, 106.
Rock, K.L., Reits, E., Neefjes, J., 2016. Present Yourself! By MHC class I and MHC class II molecules. Trends Immunol. 37, 724–737.
Roszer, T., 2015. Understanding the mysterious M2 macrophage through activation markers and effector mechanisms. Mediators Inflamm. 2015, 816460.
Saederup, N., Cardona, A.E., Croft, K., Mizutani, M., Cotleur, A.C., Tsou, C.L., Ransohoff, R.M., Charo, I.F., 2010. Selective chemokine receptor usage by central nervous system myeloid cells in CCR2-red fluorescent protein knock-in mice. PLoS ONE 5, e13693.
Schulz, C., Gomez Perdiguero, E., Chorro, L., Szabo-Rogers, H., Cagnard, N., Kierdorf, K., Prinz, M., Wu, B., Jacobsen, S.E., Pollard, J.W., Frampton, J., Liu, K.J., Geissmann, F., 2012. A lineage of myeloid cells independent of Myb and hematopoietic stem cells. Science 336, 86–90.
Shu, R., Bai, D., Sheu, T., He, Y., Yang, X., Xue, C., He, Y., Zhao, M., Han, X., 2017. Sclerostin promotes bone remodeling in the process of tooth movement. PLoS ONE 12, e0167312.
Smith, T.D., Tse, M.J., Read, E.L., Liu, W.F., 2016. Regulation of macrophage polarization and plasticity by complex activation signals. Integr. Biol. (Camb.) 8, 946–955.
Stansley, B., Post, J., Hensley, K., 2012. A comparative review of cell culture systems for the study of microglial biology in Alzheimer's disease. J. Neuroinflammation 9, 115.
Stoppini, L., Buchs, P.A., Muller, D., 1991. A simple method for organotypic cultures of nervous tissue. J. Neurosci. Methods 37, 173–182.
Takata, K., Kozaki, T., Lee, C.Z.W., Thion, M.S., Otsuka, M., Lim, S., Utami, K.H., Fidan, K., Park, D.S., Malleret, B., Chakarov, S., See, P., Low, D., Low, G., Garcia-Miralles, M., Zeng, R., Zhang, J., Goh, C.C., Gul, A., Hubert, S., Lee, B., Chen, J., Low, I., Shadan, N.B., Lum, J., Wei, T.S., Mok, E., Kawanishi, S., Kitamura, Y., Larbi, A., Poidinger, M., Renia, L., Ng, L.G., Wolf, Y., Jung, S., Onder, T., Newell, E., Huber, T., Ashihara, E., Garel, S., Pouladi, M.A., Ginhoux, F., 2017. Induced-pluripotent-stem-cell-derived primitive macrophages provide a platform for modeling tissue-resident macrophage differentiation and function. Immunity 47 183–198 e186.
Timmerman, R., Burm, S.M., Bajramovic, J.J., 2018. An overview of in vitro methods to study microglia. Front. Cell. Neurosci. 12, 242.
Varvel, N.H., Neher, J.J., Bosch, A., Wang, W., Ransohoff, R.M., Miller, R.J., Dingledine, R., 2016. Infiltrating monocytes promote brain inflammation and exacerbate neuronal damage after status epilepticus. Proc. Natl. Acad. Sci. USA 113, E5665–E5674.
Vinet, J., Weering, H.R., Heinrich, A., Kalin, R.E., Wegner, A., Brouwer, N., Heppner, F.L., Rooijen, N., Boddeke, H.W., Biber, K., 2012. Neuroprotective function for ramified microglia in hippocampal excitotoxicity. J. Neuroinflammation 9, 27.
Yamasaki, R., Lu, H., Butovsky, O., Ohno, N., Rietsch, A.M., Cialic, R., Wu, P.M., Doykan, C.E., Lin, J., Cotleur, A.C., Kidd, G., Zorlu, M.M., Sun, N., Hu, W., Liu, L., Lee, J.C., Taylor, S.E., Uehlein, L., Dixon, D., Gu, J., Floruta, C.M., Zhu, M., Charo, I.F., Weiner, H.L., Ransohoff, R.M., 2014. Differential roles of microglia and monocytes in the inflamed central nervous system. J. Exp. Med. 211, 1533–1549.
Zeger, S.L., Liang, K.Y., Albert, P.S., 1988. Models for longitudinal data – a generalized estimating equation approach. Biometrics 44, 1049–1060.
Zhuang, L., Pound, J.D., Willems, J.J., Taylor, A.H., Forrester, L.M., Gregory, C.D., 2012. Pure populations of murine macrophages from cultured embryonic stem cells. Application to studies of chemotaxis and apoptotic cell clearance. J. Immunol. Methods 385, 1–14.